

The VIMOS Ultra-Deep Survey: evidence for AGN feedback in galaxies with CIII]- λ 1908Å emission 10.8 to 12.5 Gyr ago [★]

O. Le Fèvre¹, B. C. Lemaux^{1,2}, K. Nakajima^{3,4}, D. Schaerer^{3,5}, M. Talia⁶, G. Zamorani⁷, P. Cassata⁵, B. Garilli⁸, D. Maccagni⁸, L. Pentericci⁹, L. A. M. Tasca¹, E. Zucca⁷, R. Amorin^{9,13}, S. Bardelli⁷, A. Cimatti⁶, M. Giavalisco¹⁰, L. Guaita⁹, N.P. Hathi¹¹, F. Marchi⁹, E. Vanzella⁷, D. Vergani⁹, and J. Dunlop¹²

¹ Aix Marseille Université, CNRS, LAM (Laboratoire d'Astrophysique de Marseille) UMR 7326, 13388, Marseille, France

² Department of Physics, University of California, Davis, One Shields Ave., Davis, CA 95616, USA

³ Geneva Observatory, University of Geneva, ch. des Maillettes 51, CH-1290 Versoix, Switzerland

⁴ European Southern Observatory, G-85748 Garching bei München, Germany

⁵ Institut de Recherche en Astrophysique et Planétologie - IRAP, CNRS, Université de Toulouse, UPS-OMP, 14, avenue E. Belin, F31400 Toulouse, France

⁶ University of Bologna, Department of Physics and Astronomy (DIFA), V.le Berti Pichat, 6/2 - 40127, Bologna

⁷ INAF-Osservatorio Astronomico di Bologna, via Ranzani, 1 - 40127, Bologna

⁸ INAF-IASF Milano, via Bassini 15, I-20133, Milano, Italy

⁹ INAF-Osservatorio Astronomico di Roma, via di Frascati 33, I-00040, Monte Porzio Catone, Italy

¹⁰ Astronomy Department, University of Massachusetts, Amherst, MA 01003, USA

¹¹ Space Telescope Science Institute, 3700 San Martin Drive, Baltimore, MD 21218, USA

¹² SUPA, Institute for Astronomy, University of Edinburgh, Royal Observatory, Edinburgh, EH9 3HJ, United Kingdom

¹³ Kavli Institute for Cosmology, University of Cambridge, Madingley Road, Cambridge, CB3

e-mail: olivier.lefevre@lam.fr

Received ...; accepted ...

ABSTRACT

We analyze the CIII]- λ 1908Å emission properties in a sample of 3899 star-forming galaxies (SFGs) at $2 < z < 3.8$ drawn from the VIMOS Ultra-Deep Survey (VUDS). We find a median equivalent width $EW(CIII)] = 2.0 \pm 0.2$ to $2.2 \pm 0.2 \text{Å}$ for the whole SFG population at $2 < z < 3$ and $3 < z < 4$, respectively. About 24% of SFGs are showing $EW(CIII)] > 3 \text{Å}$, including $\sim 20\%$ with modest emission $3 < EW(CIII)] < 10 \text{Å}$ and $\sim 4\%$ with strong emission $EW(CIII)] > 10 \text{Å}$. A small but significant fraction of 1.2% of SFGs presents strong CIII] emission $20 < EW(CIII)] < 40 \text{Å}$, with the four strongest emitters ($EW(CIII)] > 40 \text{Å}$ up to $\sim 95 \text{Å}$) being associated with broad-line quasars. While this makes CIII] the second most-frequent emission line in the UV rest-frame spectra of SFGs after Ly α , this line alone cannot be considered an efficient substitute to measure a galaxy redshift in the absence of Ly α emission, unless the spectral resolution is $R > 3000$ to distinguish among different possible doublets. We find a large dispersion in the weak correlation between $EW(CIII)]$ and $EW(Ly\alpha)$, with galaxies showing strong CIII] and no Ly α , and vice-versa. The spectra of SFGs with $10 < EW(CIII)] < 40 \text{Å}$ present strong emission lines including CIV- λ 1549, HeII- λ 1640, OIII- λ 1664, but also weaker emission features of highly ionized elements like SiIV- λ 1403, NIV- λ 1485, NIII- λ 1750, or SiIII- λ 1888, indicating the presence of a hard radiation field. We present a broad range of observational evidence supporting the presence of AGN in the strong CIII] emitting population. As $EW(CIII)]$ is rising, we identify increasingly powerful outflows with velocities up to $\sim 1014 \text{ km/s}$, beyond what stellar winds are commonly producing. The strongest CIII] emitters are preferentially located below the main sequence of star-forming galaxies, with the median star formation rate being reduced by a factor of two. In addition, we find that the median stellar age of the strongest emitters is $\sim 0.8 \text{ Gyr}$, about three times that of galaxies with $EW(CIII)] < 10 \text{Å}$. X-ray stacked imaging of the strong CIII] emitters sample show a marginal 2σ detection consistent with low luminosity AGN $\log(L_X(2 - 10 \text{ keV})) \sim 42.9 \text{ erg/s}$. Spectral line analysis and classification presented in a joint paper by Nakajima et al. (2017) confirms that the strongest emitters require the presence of an AGN. We conclude that these properties are indicative of AGN feedback acting in SFGs at $2 < z < 3.8$, contributing to star-formation quenching. We find that quenching timescales of $\sim 0.25 - 0.5 \times 10^9$ years, are necessary for such AGN feedback to turn part of the star-forming galaxy population with $M_{star} > 10^{10} M_\odot$ at $z \sim 3$ into the population of quiescent galaxies observed at redshift $z \sim 1 - 2$.

Key words. Galaxies: high redshift – Galaxies: evolution – Galaxies: formation – Galaxies: star formation – Galaxies: active galactic nuclei

1. Introduction

Progress in understanding the formation and early assembly of galaxies requires assembling large samples of high redshift

galaxies. The first galaxies formed during the epoch of reionization (EoR) are thought to contribute most of the photons transforming neutral Hydrogen into a fully ionized medium at $z > 6$ (Robertson et al. 2015). However, this evidence is based mostly on a census of galaxies identified from their photometric properties (e.g. Bouwens et al. 2015), while confirming their redshift remains difficult because spectral signatures allowing their iden-

[★] Based on data obtained with the European Southern Observatory Very Large Telescope, Paranal, Chile, under Large Program 185.A-0791.

tification are scarce (Pentericci et al. 2011; Stark et al. 2010). Transforming the large population of galaxy candidates at $z > 6$ into reference samples with the confirmed spectroscopic redshifts needed to infer their physical properties remains a major issue.

In the rest-frame UV spectra of galaxies observed at these redshifts, several spectral features are expected to be present, but only a few emission lines may reach a sufficient strength to be detected and either serve as a useful reference for a robust redshift measurement, or as a physical diagnostic to the ionizing field and interstellar medium (ISM). The properties of these lines need to be well understood to make progress in finding and characterizing galaxies at these redshifts.

The main spectral features used to identify distant galaxies rely on the properties of the Hydrogen atom between the Lyman- α (hereafter $Ly\alpha$) transition at $\lambda 1215.7\text{\AA}$ and the Lyman limit at $\lambda 912\text{\AA}$. While the Lyman-limit and continuum dropout from absorption by gas clouds in the inter-galactic medium (IGM) on the line of sight allow the identification of candidate high redshift galaxies from photometry alone, the key feature allowing to robustly identify distant galaxies from spectroscopic follow-up is the $Ly\alpha$ emission, primarily produced by gas photo-ionized by young hot stars. $Ly\alpha$ emission, when present, is easier to detect than a continuum break and therefore most of the galaxies at $z > 6$ securely confirmed from spectroscopy today are based on the detection of $Ly\alpha$ in emission. Narrow-band imaging is also used for $Ly\alpha$ emitters searches (e.g. Ouchi et al. 2008), but it remains difficult to analyze extreme populations like strong emitters appearing as massive, old, and with low star formation (Taniguchi et al. 2015) without additional spectral information besides $Ly\alpha$.

Unfortunately, it appears that the fraction of $Ly\alpha$ emitters, while rising up to $z \sim 6$ (e.g. Stark et al. 2009; Cassata et al. 2015; De Barros et al. 2017), seems to be suddenly decreasing at higher redshifts, which is interpreted as the signature of the end of reionization at around $z \sim 6$ (Stark et al. 2010; Pentericci et al. 2014). Neutral Hydrogen acts to significantly scatter $Ly\alpha$ which diffuses the emission, and, in the presence of dust, causes attenuation which makes the feature difficult to detect at $z > 6$ (Vanzella et al. 2011; Treu et al. 2013; Pentericci et al. 2014; Oesch et al. 2016; Hoag et al. 2017). One is therefore seeking alternatives to $Ly\alpha$ to obtain accurate redshift measurements of the most distant galaxies.

Interestingly, the Carbon line emission may come to the rescue, from atomic transitions visible both in the sub-millimeter domain with the [CII]- $158\mu\text{m}$ line (e.g. Carilli & Walter 2013; Capak et al. 2015; Pentericci et al. 2016; Bradač et al. 2017), as well as in the UV rest-frame domain with the CIII] emission at $\lambda \sim 1908\text{\AA}$, combined with the more complex CIV- $\lambda 1549$ feature, observed both in emission from photo-ionization processes and in absorption (Schmidt et al. 2017). In the UV rest-frame the HeII- $\lambda 1640\text{\AA}$ line is also expected to be present as a tracer of the first stellar populations like PopIII present only on short timescales of a few million years (e.g. Schaerer 2003; Cassata et al. 2013; Sobral et al. 2015), or from young stellar populations (Cassata et al. 2013; Kehrig et al. 2015).

The CIII]- $\lambda 1908$ emission was recently proposed as an alternative to $Ly\alpha$ to identify distant galaxies for which there is no $Ly\alpha$ in emission (Stark et al. 2014). At intermediate redshifts, CIII] emission has been reported starting with the first large spectroscopic census of LBGs (Shapley et al. 2003). At these redshifts, this line seems to be more prominent for low-mass systems, and may be correlated to $Ly\alpha$ (Stark et al. 2014).

Several studies report CIII] emission at $2 < z < 4$, either from individual galaxies (Erb et al. 2010; Talia et al. 2012; Karman et al. 2014; Steidel et al. 2014), or in high signal-to-noise stacks (Shapley et al. 2003), independently of whether $Ly\alpha$ is in emission or not (Le Fèvre et al. 2015). At $z > 6$ CIII] is now reported in the observed spectra of several galaxies (Stark et al. 2015), but absent in others (Sobral et al. 2015; Schmidt et al. 2016) with solid upper limits (Shibuya et al. 2017). However, the prevalence of CIII] emitters is as yet unknown and a robust reference to the properties of low to intermediate redshift analogs to the high redshift CIII] emitters is therefore needed for this line to be useful in analyzing star-forming galaxies at the highest redshifts (Rigby et al. 2015; Du et al. 2016; Stroe et al. 2017; Amorín et al. 2017).

The CIII]- $\lambda 1908$ emission offers an interesting opportunity for a diagnostic of the physical conditions in distant star-forming galaxies. It is a doublet, combination of [CIII]- $\lambda 1907\text{\AA}$, a forbidden magnetic quadrupole transition and CIII]- $\lambda 1909$, a semi-forbidden electro-dipole transition (Stark et al. 2014), with a critical density $N_e \approx 10^{10} \text{cm}^{-3}$ and requiring an ionizing potential of 24.4 eV. In star-forming galaxies the strong ionizing flux produced by young hot stars may be sufficient to photo-ionize Carbon with the production of CIII] photons. The strong ionizing background produced by active galactic nuclei (AGN) also leads to the ubiquitous CIII] emission observed in quasar spectra (Vanden Berk et al. 2001). Strong CIII] emission with an equivalent width $EW(\text{CIII])}$ in excess of 20\AA can mainly be produced by the hard ionizing spectrum of an AGN, or, in exceptional cases, by extreme stellar populations, as described in Nakajima et al. (2017). Sufficient ionizing flux may also arise in the presence of shocks, e.g. produced by SNe, jets from a radio-source (e.g. Best et al. 2000), or from gas compression during a merger event (Bournaud et al. 2011). Characterizing the source of CIII] emission can therefore provide important clues on the star formation and the co-evolution with AGN, and in particular the possibility of AGN activity quenching star formation, a mechanism proposed to evolve star-forming galaxies at high- z into quiescent galaxies at $z \sim 1-2$ and below (Silk & Rees 1998) (for a recent account see e.g. Barro et al. 2013; Dubois et al. 2013).

In this paper we seek to characterize the prevalence and properties of CIII]- $\lambda 1908$ emitters in the general star-forming galaxy population at redshifts $2 < z < 3.8$ using rest-frame UV spectra obtained from the large VIMOS Ultra Deep Survey (VUDS, Le Fèvre et al. 2015). The large sample of 3899 galaxies with the most reliable redshift measurements in VUDS, representative of the star-forming galaxy population at these redshifts, enables for the first time to establish the distribution and properties of the CIII] emission 10.8 to 12.5 Gyr back in cosmic time.

We summarize the VUDS survey properties relevant for CIII] observations in Sect.2, and present the methodology to measure CIII] equivalent width and flux together with examples of individual CIII] emitters of different strengths. The average spectral properties of the different CIII] populations are described in Sect.3, including an attempt to identify the contribution from AGN. The $Ly-\alpha$ properties of CIII] emitters are discussed in Sect.4. We derive the equivalent width distribution of CIII] emitters and the CIII] emitters fraction among young star-forming galaxies in Sect.5. We discuss the general observed properties of the CIII] emitters in Sect.6 including their position on the $SFR-M_{star}$ plane. Evidence for AGN feedback quenching star-formation is presented in Sect.7. A summary is provided in Sect.8.

The data presented in this paper are further analyzed in light of a wide grid of photoionization models, as discussed by Nakajima et al. (2017).

When quoting absolute quantities we use a cosmology with $H_0 = 70 \text{ km s}^{-1} \text{ Mpc}^{-1}$, $\Omega_{0,\Lambda} = 0.7$ and $\Omega_{0,m} = 0.3$. All magnitudes are given in the AB system. We use a definition of equivalent width with positive values indicating emission and negative values indicating absorption. All equivalent width measurements are given in the rest frame.

2. CIII]- λ 1908Å emission in VUDS

2.1. Detecting CIII] in the VUDS spectra

Spectra of $\approx 10\,000$ objects have been obtained for VUDS to study galaxy evolution in the redshift range $2 < z < 6+$. The reader is referred to Le Fèvre et al. (2015) for a detailed description of the survey observations, and methods applied to process the data and measure key parameters, including the spectroscopic redshift z_{spec} , as well as Tasca et al. (2017) for a description of the VUDS-DR1 first data release.

The key element of this sample is that the spectroscopic targets are mainly selected based on their photometric redshifts which satisfy $z_{phot} + 1\sigma \geq 2.4$ and $i_{AB} \leq 25$, with a well-defined selection of objects. The wavelength range of the final spectra is $3600 < \lambda < 9350\text{Å}$, cumulating 14h integrations in each of the LRBLUE and LRRED grisms of the VIMOS spectrograph on the ESO Very Large Telescope (Le Fèvre et al. 2003), with a spectral resolution $R \sim 230$.

Standard data processing is performed using the VIPGI environment (Scodreggio et al. 2005), followed by redshift measurement using the EZ package (Garilli et al. 2010). The target selection produces a final VUDS sample representative of the star-forming galaxy population in the redshift range $2 < z < 6.5$, flux-selected from the rest-frame continuum UV luminosity. An important aspect of the VUDS is the wide field (large volume) covered. A total of 1 deg^2 is covered in three fields including the COSMOS, ECDFS and VVDS-02h fields. This enables to reduce cosmic variance in the redshift range of interest, to below 10% (Moster et al. 2011). We identify galaxies with Ly α in emission as well as in absorption (Le Fèvre et al. 2015, e.g. Figure 19 and 20), and the fraction of Ly α emitters with $EW(\text{Ly}\alpha) > 25\text{Å}$ in the redshift range of this study is $\sim 11\%$ (Cassata et al. 2015).

The instrumental setup translates to the ability to follow the CIII] line reliably from a redshift $z = 2$ up to $z \approx 3.8$. At the spectral resolution of the observations, the CIII] λ 1907–1909 doublet is not resolved, and for the remainder of this paper, we will refer to the doublet simply as CIII]- λ 1908, or CIII]. The ability to identify CIII] varies with the observed wavelength in a non-linear way, as the line will appear on top or in-between the strong night-sky OH emission. This aspect is further discussed below. All other lines bluer than CIII] and redder than Ly α useful for spectral diagnostics can be followed for $2 < z < 3.8$. We are therefore restricting the VUDS sample to the 3899 galaxies observed in the redshift range $2 < z < 3.8$, with spectroscopic redshift measurements going from reliable (flag 2 and 9, $\sim 80\%$ probability of being right) to very reliable (flag 3, 4, $\sim 100\%$ probability of being right, Le Fèvre et al. 2015).

A large range of ancillary data is available for galaxies in VUDS, with physical parameters obtained from spectral energy distribution (SED) fitting of the multi-wavelength photometric data (Tasca et al. 2015; Thomas et al. 2017), including stellar mass, star formation rate, dust extinction E(B-V), age,

or metallicity. The possible presence of obscured AGN in the sample, with an obscured view of the central engine, is not expected to strongly contribute to the overall UV continuum (e.g. Bundy et al. 2008; Assef et al. 2010; Hainline et al. 2012). The physical properties of galaxies derived from SED-fitting using templates which do or do not include an obscured AGN component are compared in Bongiorno et al. (2012) who find little differences on stellar masses and star formation rates. Galaxy sizes used in this study are drawn from those measurements reported in Ribeiro et al. (2016b) and we also draw on the morphology analysis of bright clumps made in Ribeiro et al. (2016a).

2.2. Measurements of CIII]- λ 1908 equivalent width and flux

The measurement of line flux and equivalent width (EW) is performed on each galaxy individually. We first measure the flux and EW of CIII] using a custom code in IDL to define the sample of CIII] emitters (following Lemaux et al. 2010). When CIII] falls in wavelength domains with moderate to strong OH sky lines, we flag galaxies for which this is the case in the following way: we raise a 'sky flag' when any such OH sky line (as given in Hanuschik 2003) falls within a 17Å bandpass defining the CIII] line (we use bandpasses of 25Å and 23Å for HeII and CIV, resp.). We then iterate manually on these measurements performing a direct line integration using the splot tool in IRAF to obtain the final measurements of EW and flux, after the identification of the continuum under CIII] evaluating the continuum level on each side of the line, and updating the automated measurement if necessary. We proceed in the same way to obtain measurements of CIV- λ 1549, HeII- λ 1640 and other lines of interest, while for Ly α we use a similar technique but perform the continuum estimate from the red side of the line only.

We estimate the median error in measuring the EW of a line as the r.m.s. uncertainty resulting from noise on the spectra as measured on each side of the line, and we typically measure $1\sigma_{median}(EW) = 1.0\text{Å}$ for all lines of interest. This results into a 3σ lower limit of 3Å on $EW(\text{CIII])}$, limited by the faintness of the sources as observed in low $R \approx 230$ resolution spectra.

For 2543 galaxies the background noise at the wavelength of CIII] is not affected by sky residuals or other instrumental defects. We find that 1763 of these galaxies have CIII] in emission, $EW(\text{CIII])} > 0$, while 429 and 120 galaxies have a signal-to-noise of the CIII] line larger than 3 and 5, respectively.

3. Average CIII] properties from stacked VUDS spectra

3.1. CIII] populations

To analyse the CIII] emitters, we arbitrarily split the VUDS sample of star-forming galaxies with $2 < z < 3.8$ and $S/N > 3$ in the following sub-samples:

- $EW(\text{CIII])} > 20\text{Å}$: the "very strong emitters" (31 galaxies)
- $10 < EW(\text{CIII])} \leq 20\text{Å}$: the "strong emitters" (109 galaxies)
- $5 < EW(\text{CIII])} \leq 10\text{Å}$: the "medium emitters" (289 galaxies)
- $0 < EW(\text{CIII])} \leq 5\text{Å}$: the "weak emitters" (1334 galaxies)
- "SFG": A UV-rest selected representative sample of 1455 star forming galaxies from VUDS (with the best reliability flags 3 and 4), including 951 with $2 < z < 3$ and 504 with $3 < z < 4$

The median EW(CIII]) for the first four categories are 27.1, 13.8, 8.0, and 3.4Å, respectively. This compares to EW(CIII]) = 2.0 ± 0.2 and 2.2 ± 0.2 Å for the whole population of UV-rest selected SFGs at $2 < z < 3$ and $3 < z < 4$, respectively.

Examples of CIII] emitters over the range of observed EW(CIII]) are presented in Figs. 1 to 3.

Individual spectra of CIII] emitters show a wide range of properties. We observe that CIII] emission occurs in galaxies with Ly α either in emission or absorption. This is further investigated in Sect. 4. The presence of CIV- λ 1549 emission indicates a substantial flux of ionizing photons with energies in excess of 47.9 eV. Depending on the spectra, and best identified in the stacks (see below), a wealth of absorption and emission lines are identified. The most common emission lines beside CIII] and Ly α are CIV- λ 1549 (a blend of CIV-1549 and CIV-1551, combining nebular emission and stellar absorption) and HeII-1640, and we also observe OIII]- λ 1663 (blend of the λ 1661-1666 doublet at the resolution of VUDS), NIII]- λ 1750, NIV- λ 1485, as well as NV- λ 1240, SiII- λ 1309, SiIII- λ 1888 and SiIV- λ 1403. In rare cases Ly β and OVI- λ 1035 are also observed in emission.

Similarly to Le Fèvre et al. (2015) we produce summed ("stacked") spectra of VUDS galaxies in the rest-frame using the VUDS catalog redshift (as described in the presentation of the first VUDS data release, Tasca et al. 2017). These stacks are produced by normalizing the continuum between 1300 and 1600Å and summing the flux from all galaxies in a given category defined above, using the `scombine` task under IRAF, with sigma clipping set at 3σ . In these stacks, we do not use objects identified as AGN, either with broad line or NV- λ 1240 emission presented in Sect. 3.2.

We find that the lower EW measurements include significant contamination from noise, that we correct to obtain the fraction of emitters as a function of EW(CIII]) as described in Sect.5. Spectra for each of the stacks are therefore selected from the complete VUDS sample galaxies but keeping only those objects with a CIII] signal to noise larger than 5, and satisfying a visual inspection such that CIII] is clear of sky subtraction residual or other spectral defect. A total of 43, 31, 30, and 16 spectra are stacked for the weak, medium, strong and very strong emitters, respectively. Stacked spectra for these different categories are shown in Fig. 4. For the "SFG" sample we do not apply any signal to noise restriction, as the sample is large enough to produce a stable stack.

The spectra show interesting features which change when EW(CIII]) is increasing: besides the Ly α properties discussed in Sect. 4, we find emission lines of several atomic species which appear and grow stronger. For the whole SFG population we observe both CIII] and HeII- λ 1640 in emission, as well as a fainter CIV- λ 1549 emission partially suppressed by strong absorption with a P-Cygni profile. Observing both CIII] and HeII in emission is expected as these two lines are ionized under similar conditions as the energy required to ionize helium is only slightly greater than the energy required to doubly-ionize carbon (24.6 vs. 24.4 eV), and faint HeII emission is frequently observed in the general population. The HeII emission presents a useful diagnostic for very young as well as more exotic stellar populations (Schaerer 2003; Cassata et al. 2013) and will be discussed in a forthcoming paper.

As EW(CIII]) increases we observe in the stacked spectra that HeII and CIV are getting stronger, interstellar medium lines like SiII- λ 1260, OI+SiII- λ 1303, CII- λ 1334, SiV- λ 1393.76-1402.8, are filling-in, OIII]- λ 1663 appears for $5 < \text{EW}(\text{CIII])} < 10$,

and NIV- λ 1645 and NIII]- λ 1750 are both visible for the $10 < \text{EW}(\text{CIII])} < 20$ stack. The combined spectrum of the strongest emitters with $\text{EW}(\text{CIII])} \geq 20$ strikingly shows a wealth of strong emission lines, as presented in Figure 5. Besides CIII], we identify the following lines in emission: NV- λ 1240, SiII- λ 1309, SiIV- λ 1403, NIV]- λ 1485, CIV- λ 1549, HeII- λ 1640, [OIII]- λ 1663, NIII]- λ 1750, SiIII]- λ 1888, with a spectrum comparable to that of the UV-selected AGN sample at $z \sim 2 - 3$ from Hainline et al. (2011). With OIII]- λ 1663, SiIII, NIII, NIV and NV requiring energy levels above 35.1, 16.3, 29.6, 47.5, and 77.5 eV, respectively, this is in line with the ionizing field in these galaxies getting stronger.

We provide measurements of EW and line flux relative to CIII] from the stacked spectra of the different CIII] populations in Table 2, and in Table 3 for the whole SFG populations at $2 < z < 3$ and $3 < z < 4$. We also indicate the slope β of the UV continuum, parametrized as $F_\lambda \propto \lambda^\beta$, measured from the continuum values between 1400Å and 2100Å rest-frame (Hathi et al. 2016). To measure these continuum values, we fit the observed continuum with a cubic spline excluding 30Å around known emission and absorption features. We observe that β is smaller (continuum steeply declining with wavelength) for the strongest CIII] emitters with $\beta = -1.76 \pm 0.06$, and gradually become flatter for populations with decreasing EW(CIII]), reaching $\beta = -0.92$ for the whole SFG population. This observation corroborates the presence of a stronger UV ionizing field for the strongest CIII] emitters.

3.2. Contribution from AGN

We make an attempt to identify the contribution of AGN to the SFG population. Four objects among the 3899 sources with $2 < z < 3.8$ meet the conditions to be classified as broad-line type-I AGN, imposing that one or more of the observed emission lines in the VUDS spectral window have $FWHM > 1000\text{km/s}$. These objects present spectra similar to broad-line quasar spectra at similar redshifts (e.g. Vanden Berk et al. 2001), as can be seen in the stacked spectrum on the bottom panel of Fig.6.

The NV- λ 1240 emission requires a strong ionizing field ~ 77 eV, and therefore has been proposed as a criterion to identify narrow line type-II AGN (e.g Hainline et al. 2011). As this criterion may not strictly be exclusive of other ionization source for weak NV emission, we search for emitters with $\text{EW}(\text{NV}) > 10\text{Å}$ which are most likely type-II AGN, and we identify seven such narrow emission line objects.

The stacked spectrum of the strong NV emitters is shown in the top panel of Fig.6. We easily identify Ly β , OVI- λ 1032, Ly α , NV- λ 1240, SiIV- λ 1403, NIV- λ 1485, CIV- λ 1549, HeII- λ 1640, OIII]- λ 1664, CIII]- λ 1908, CII]- λ 2326, [NeIV]- λ 2424, in emission. The CIV/CIII] flux ratio for these VUDS narrow-line AGN range from 1.2 to 4.7 with a median CIV/CIII] = 2.7. This ratio is lower than the class A composite spectrum of type II quasars presented in Alexandroff et al. (2013) with CIV/CIII] = 7.5. However, it is higher than the sample of type II AGN in Hainline et al. (2011) for which CIV/CIII] \sim 1.3, rather consistent to that of radio-galaxies at similar redshifts (Villar-Martin et al. 1997; Stern et al. 1999; Matsuoka et al. 2009), is higher than SFGs which have a typical ratio below unity (Nakajima et al. 2017).

Some contribution to the CIV- λ 1549, SiIV- λ 1403 and NV- λ 1240 may be coming from stellar winds produced by strong star formation. Studying a sample of local analogs to high- z Lyman break galaxies Heckman et al. (2011) indicate that a

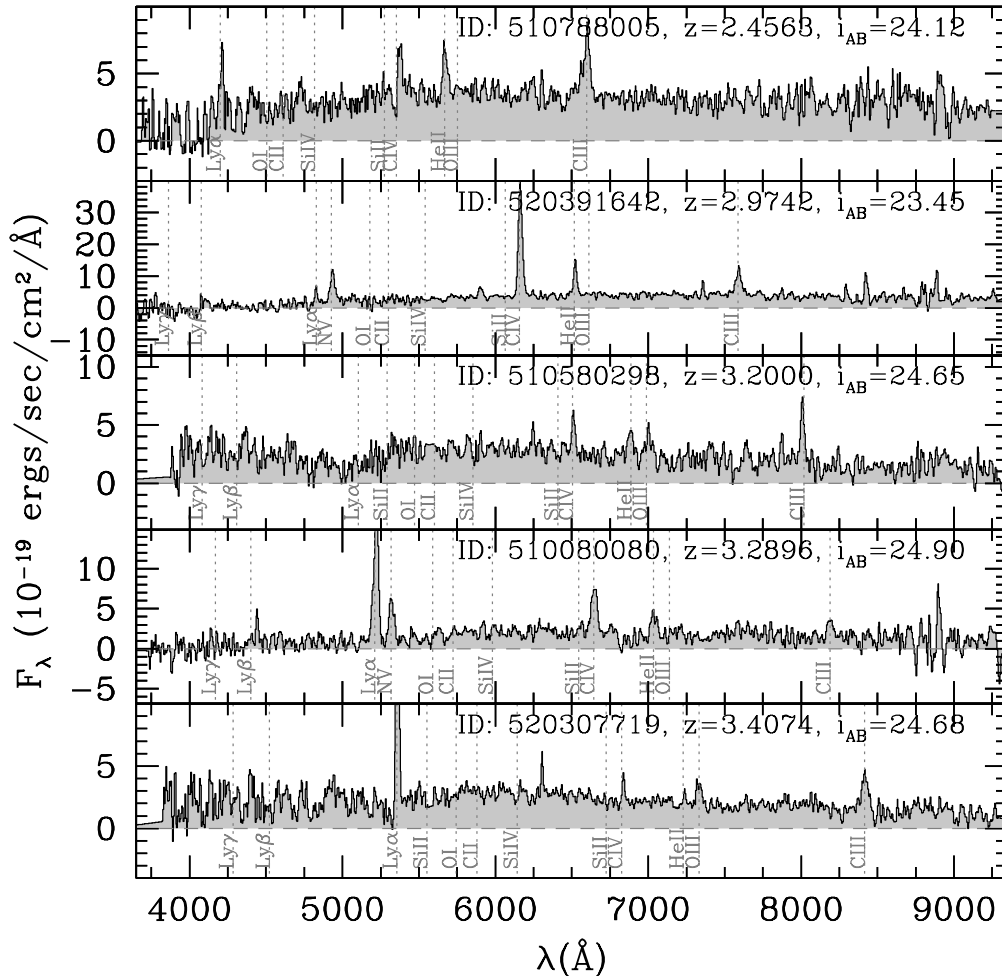


Fig. 1. Example VUDS spectra of CIII]- λ 1908 emitters with very strong EW(CIII)] $\geq 20\text{\AA}$. Note the diversity of strong CIII] emitters spectra, including strong Ly- α emission as well as weak Ly- α emission (ID:510788005 and ID:510580298).

broad NV- λ 1240 line, with a P-cygni profile, could arise from stellar winds produced by hot (O) stars. Still only a few galaxies have CIV/CIII] values comparable to even the lowest values among the NV-detected galaxies, making a pure star formation interpretation unlikely to be correct at these low redshifts.

Interestingly two out of seven strong NV emitters show weak or absent Ly α emission (see object 520391642 in Fig.1). These two objects present a red UV continuum (β slope +2.3 and +0.8) and may therefore have dusty ISM conditions which are preventing Ly α to escape. The AGN type II stack has a much redder continuum slope $\beta = +0.2 \pm 0.05$ compared to the CIII]-selected star forming populations discussed in Sect.3.1 with $\beta > -1.6$. These results are in line with those presented by Hainline et al. (2011). This indicates that the internal extinction is stronger in the AGN population, and that a combination of a dust-obscured AGN and star formation component may combine to produce the observed spectra.

We note that the AGN sample we have identified here based on NV are almost certainly, as we shall see later, a small subset of the total AGN population. The criteria to identify type II AGN from UV-rest spectra vary from sample to sample in the literature, and we point out the necessity to perform a quantitative spectral line analysis rather than an empirical classification. This

is developed in Nakajima et al. (2017) where various diagnostic diagrams using UV emission lines and based on photoionization models are discussed, and in particular pointing to the need of using different line ratios to separate star formation from AGN. Nakajima et al. (2017) claim that the population of strong and very strong CIII] emitters presented here must include AGN to explain the high EW(CIII)] and the location of these galaxies in diagnostic diagrams using observed UV line ratios. This is further discussed in Sect.6 and 7.

We searched for individual X-ray counterparts of CIII] emitters using Chandra observations in the CDFS (the 7 Ms catalog of Luo et al. 2017), in COSMOS (the Legacy catalog of Civano et al. 2016; Marchesi et al. 2016), and the XMM data in the VVDS-02h field (the XMM-LSS catalog of Chiappetti et al. 2013), with flux limits $L_X(2-10\text{keV})$ ranging from 3×10^{42} , to 3×10^{44} erg/s at $z \sim 3$. We found a total of 8 X-ray counterparts, one in CDFS (id #530029221), 6 in COSMOS (ids #510080080, 510788005, 511707398, 510793659, 510164473, and 5121237451) and one in the VVDS-02h (id #520426550) (see also Talia et al. 2017). These sources have X-ray luminosity in the range $43.8 < \log(L_X(2-10\text{keV})) < 44.5$. All of these objects are identified as AGN following the NV analysis described above, except one (id #510788005) which is identi-

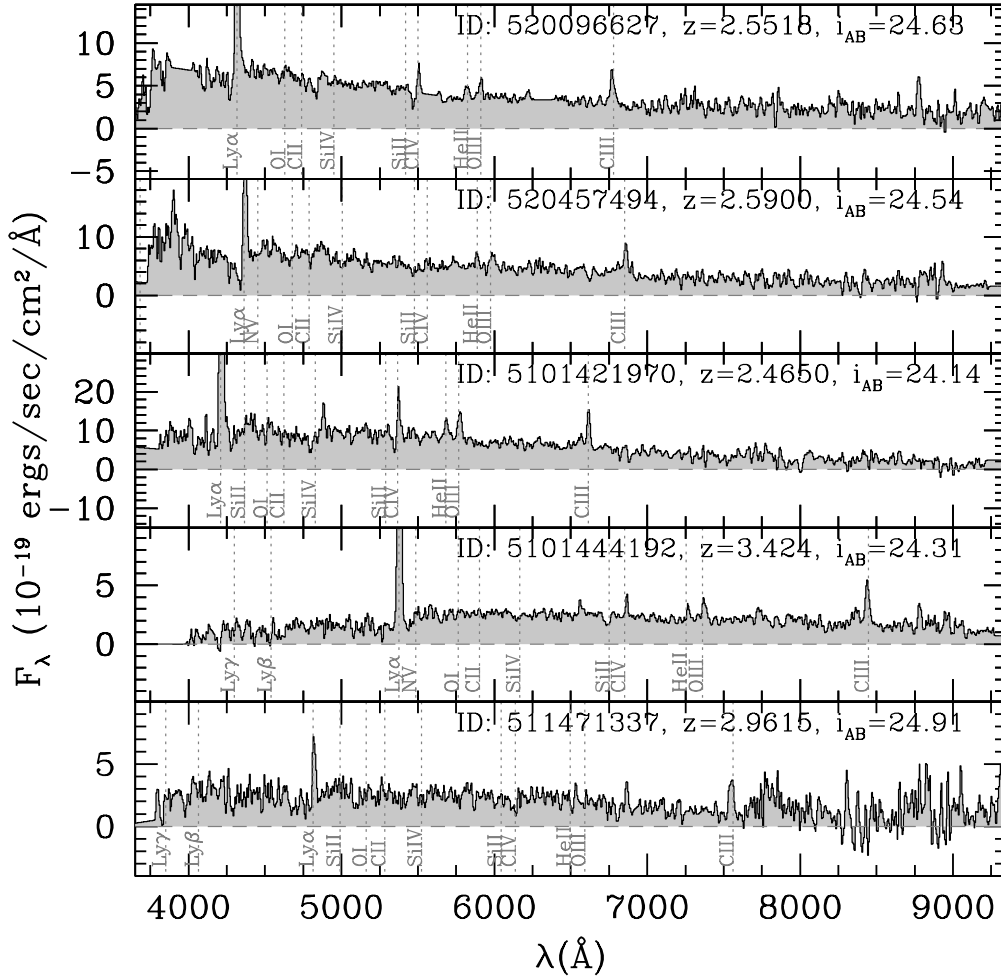


Fig. 2. Example VUDS spectra of strong CIII]1908 emitters with $10 < \text{EW}(\text{CIII])} < 20 \text{Å}$.

fied in the strong CIII] emitters list. We then performed X-ray stacking analysis on the list of strong and very strong emitters in the COSMOS field using the maps and source catalog of Civano et al. (2012). We used the the CSTACK tool to separately stack the sources in the very strong and strong CIII] emitters lists after excluding the two objects with an individual detection. In the stack of galaxies in the very strong sample the corresponding mean count rate per galaxy implies $\log L_x(2-10\text{keV}) \sim 42.6 \text{ erg/s}$ at $z \sim 3$, with a noise level in the map of $\log L_x(2-10\text{keV}) \sim 42.7 \text{ erg/s}$, meaning no significant detection. Conversely, in the strong sample there is a 2σ detection with a count rate implying $\log L_x(2-10\text{keV}) \sim 42.9 \text{ erg/s}$, with a noise level in the map of $\log L_x(2-10\text{keV}) \sim 42.6 \text{ erg/s}$. The current X-ray imaging is then not deep enough to firmly confirm the presence of an X-ray source. However, the tentative 2σ detection indicates that X-ray imaging is consistent with the very strong and strong CIII] emitting galaxies hosting low-luminosity AGN with X-ray luminosity as observed on the faint end of the AGN luminosity function at these redshifts (Georgakakis et al. 2015).

4. Lyman- α properties of CIII] emitters

We investigate the relationship between CIII] and Ly α emission in Figure 7 using the sample of CIII] emitters with $S/N > 5$.

Looking at the relation between CIII] and Ly α from the spectral stacks (Tab.2), we find a strong correlation with a Pearson correlation coefficient $r_p = 0.99$ and Spearman rank correlation coefficient $r_s = 1$ (r_p or r_s equal to one indicate a perfect one to one correlation). However, from the individual emitters, while we observe a trend for the strongest CIII] emitters to also tend to be strong Ly α emitters with a correlation significant at about the 3σ level (Student t-test), this correlation has a large dispersion. This correlation further weakens when restricting the sample of CIII] emitters to $\text{EW}(\text{Ly}\alpha) < 50 \text{Å}$ with $r_p = 0.2$, similarly to that noted by Rigby et al. (2015).

The analysis of individual emitters demonstrates that the presence of Ly α in emission increases the probability of detecting CIII], but that strong Ly α emission does not necessarily mean strong CIII] emission, or vice-versa. There are indeed numerous examples of galaxies with CIII] in emission and no or weak Ly α emission (some are presented in Fig.1 and Fig.3). We reach similar conclusions when looking at the CIV- λ 1549 line versus Ly α emission.

This behavior is somewhat expected as the radiative transfer of Ly α or CIII] photons is markedly different. As a striking example we point to object 520391642 (second from top in Figure 1) which shows strong CIII] ($\text{EW} > 20$), as well as CIV, HeII or NV, but only weak Ly α emission. Our results compare

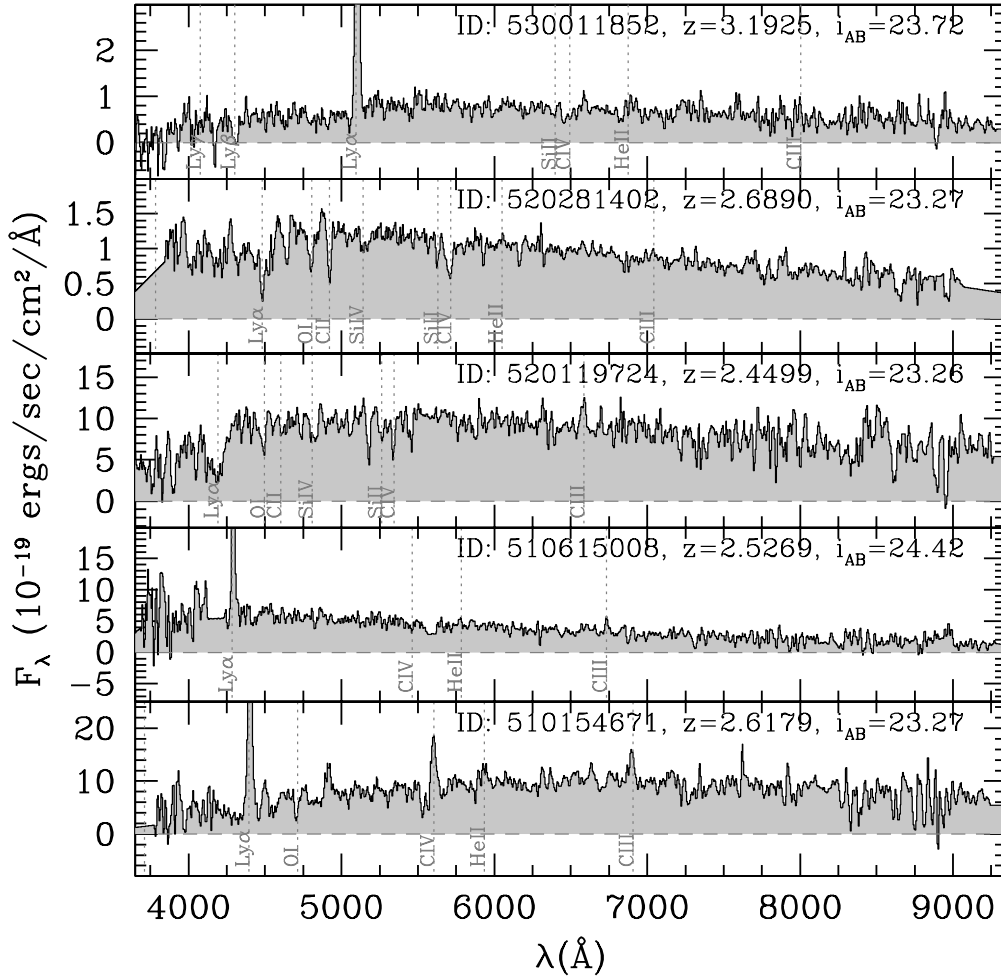


Fig. 3. Example VUDS spectra of weak CIII]1908 emitters with $0 < EW(CIII)] < 5\text{\AA}$.

well with the literature once the large spread of the relation between $EW(CIII)]$ and $EW(Ly\alpha)$, the selection, and the size of different samples, is taken into account. Looking at the average properties from stacks, our results agree well with Shapley et al. (2003). VUDS galaxies span a broad range of properties, including galaxies with and without $Ly\alpha$ in emission, expanding from smaller and possibly biased samples for which a stronger correlation between $Ly\alpha$ and CIII] is reported (Stark et al. 2014, 2015; Rigby et al. 2015; Guaita et al. 2017).

We find that galaxies with $EW(Ly\alpha) > 25$ (the definition of a $Ly\alpha$ emitter, LAE), have a 42% and 20% chance to be emitting CIII] and CIV at an appreciable level ($EW > 3\text{\AA}$), respectively. For those galaxies emitting both $Ly\alpha$ and CIII] at these levels, the median $EW(CIII)]$ is 7.7\AA as compared to a median $EW(CIV)$ of 3.4\AA for the average LAE emitting CIV.

5. Distribution of $EW(CIII)]$

To answer the question of how frequently CIII] emission is observed in UV-selected galaxies, we seek to establish the fraction of CIII] emitters in the VUDS sample as a function of $EW(CIII)]$. While it is straightforward to identify strong CIII] emitters it is more difficult to separate weak emitters from noise. We therefore proceed with a statistical analysis of the distribu-

tion of CIII] emission for the 3899 VUDS galaxies with $2 < z < 3.8$.

If CIII] emission is absent and in the presence of noise, the line measurement resulting from the process presented in Sect. 2.2 could result on either a false positive or negative EW. As CIII] is only expected in emission, we use the distribution of EW measurements indicating absorption as an estimate of how many CIII] emission lines could be produced from noise spikes, under the assumption of a Gaussian noise distribution. We compute the distribution for $EW(CIII)] < 0$, make the EW of this distribution positive (emission), and subtract this distribution from the distribution of $EW(CIII)] > 0$ to statistically correct the distribution of $EW(CIII)]$ for false CIII] emission measurements and obtain the EW distribution for CIII] emitters. For each EW bin we compute the associated error from the quadratic sum of the observed numbers of emitters and non-emitters.

The resulting rest-frame $EW(CIII)]$ distribution is shown in Figure 8, presented as the fraction of emitters with a given $EW(CIII)]$ over the full population of UV-selected star-forming galaxies, both differential and cumulative. The fraction of emitters decreases from a peak at low EW down to the largest narrow line emission galaxies with $EW(CIII)] \sim 40\text{\AA}$, as expected. We find that the population of star-forming galaxies contains $4.0 \pm 1.2\%$ of strong emitters with $EW(CIII)] > 10\text{\AA}$, including

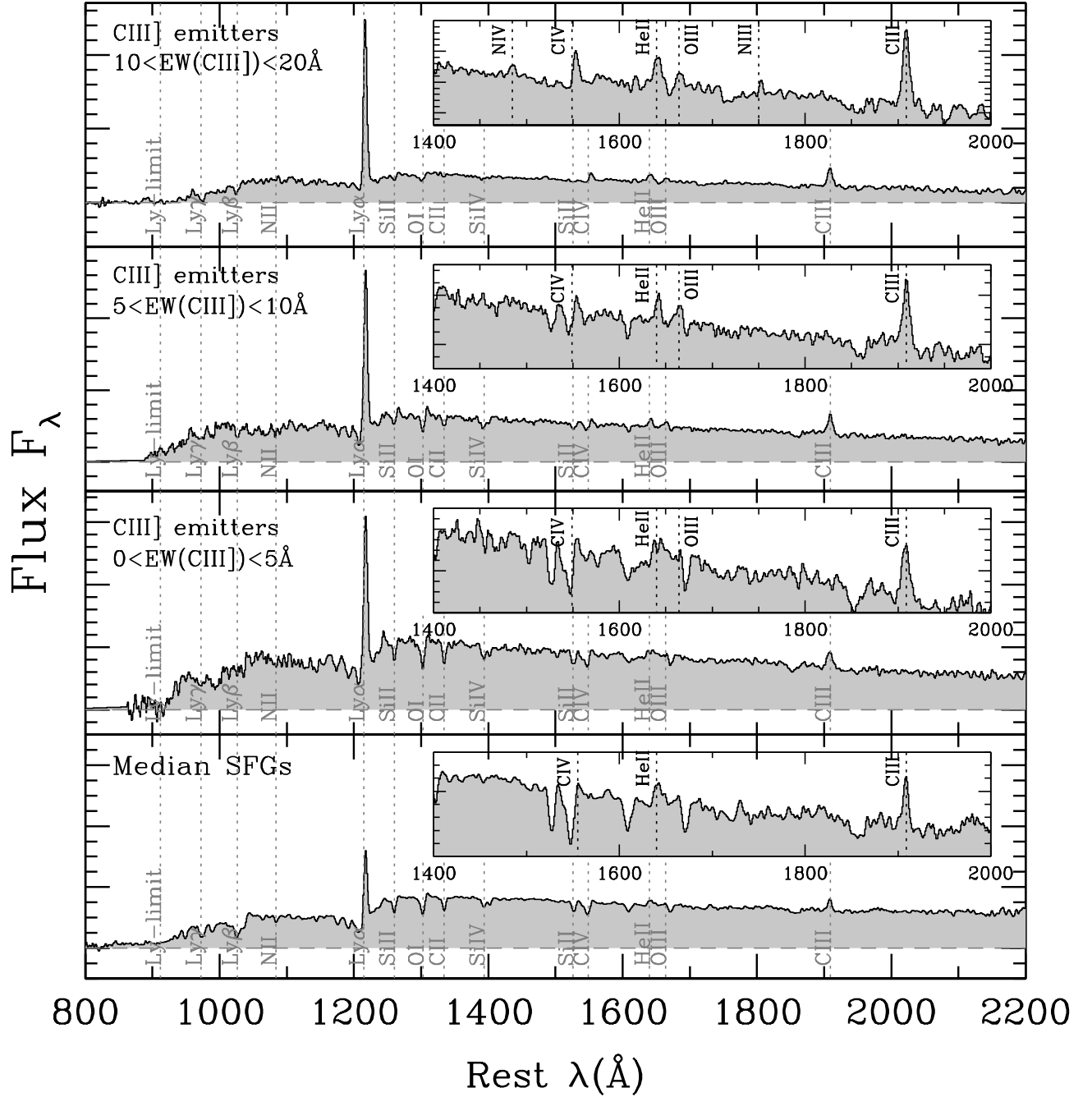


Fig. 4. Composite spectra of CIII]1908 emitters identified in the VUDS survey at $2 < z < 3.8$. From top to bottom: stack of 43 emitters with $10 < EW(CIII]) < 20$, 31 emitters with $5 < EW(CIII]) < 10$, 30 emitters with $0 < EW(CIII]) < 5$, and, for comparison, a stack of 450 galaxies representative of the general SFG population in the redshift range $2.8 < z < 3.8$.

$1.2 \pm 0.4\%$ of very strong CIII] emitters with $EW(CIII]) > 20\text{\AA}$, and $20 \pm 3.1\%$ of weak emitters $3 < EW(CIII]) < 10\text{\AA}$. The line emission distribution shows that CIII] emission is present above $EW(CIII])=3\text{\AA}$ for less than one fourth of UV star-forming galaxies at $z \sim 3$.

Besides Ly α , the CIII] line remains the most frequent emission line observed at $EW > 3\text{\AA}$. By comparison a similar analysis shows that about 10% of the galaxies emit CIV at a level $EW(CIV) > 3\text{\AA}$ sufficient to claim detection from VUDS spectra.

6. Properties of CIII] emitters

6.1. L_{NUV} , M_{star} , SFR, morphology, of CIII] emitters

In this section we compare the population of CIII] emitters to the general properties of the star-forming galaxy population. We present the relation between the rest-frame near UV luminosity L_{NUV} , the SFR, M_{star} , SSFR, and total size r_{tot} , as a function of $EW(CIII])$ in Fig.9, including the significance of the correlation using the Pearson correlation coefficient r_P and Student t-test significance.

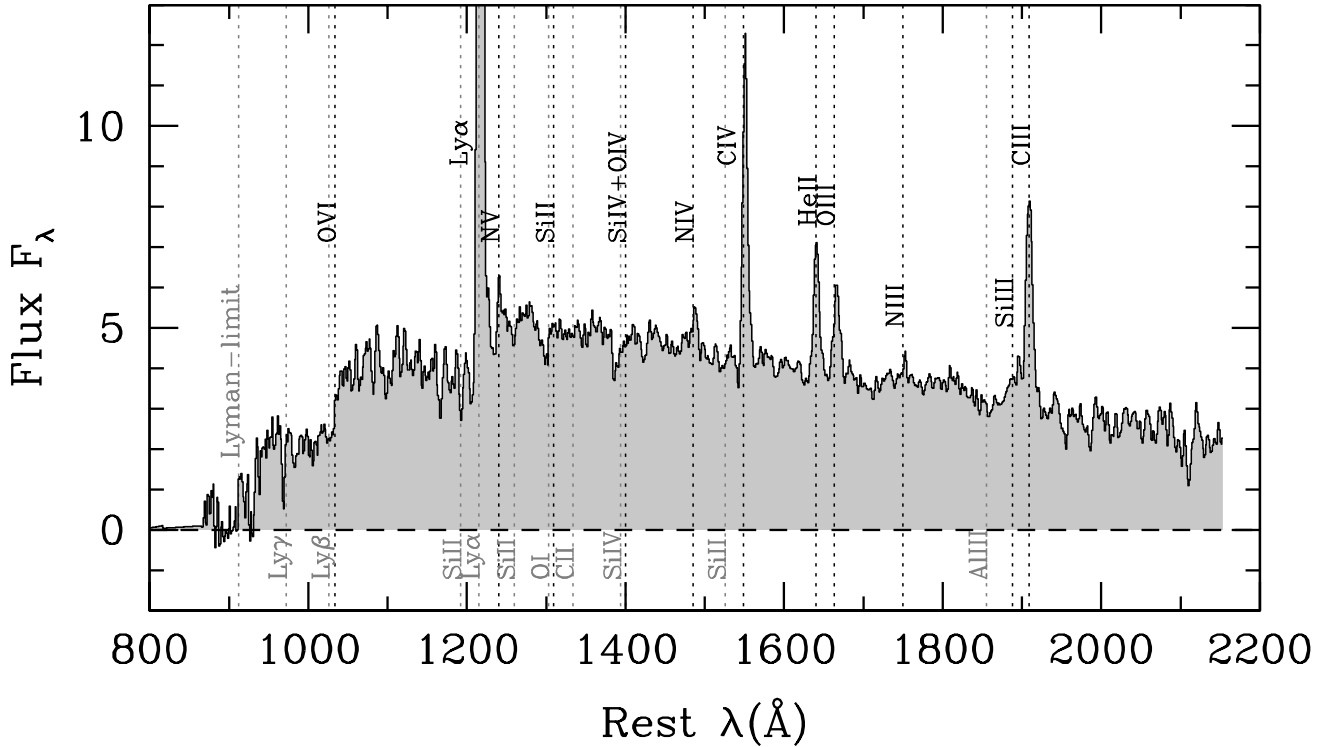


Fig. 5. Composite spectrum of 16 CIII]- λ 1908 emitters identified in the VUDS survey at $2 < z < 3.8$, with CIII] detected in emission with $S/N > 5$ and $EW(CIII)] > 20\text{\AA}$. The main emission lines associated to CIII]- λ 1908 emission can be identified as: Ly α , NV- λ 1240, NIV]- λ 1485, CIV]- λ 1549, HeII- λ 1640, OIII]- λ 1663, NIII]- λ 1750, SiIII]- λ 1888.

We find that the L_{NUV} luminosity is decreasing with increasing $EW(CIII)]$, from a median $\bar{L}_{NUV}=10.2$ in $5 < EW(CIII)] < 20$ to $\bar{L}_{NUV}=9.9$ for $EW(CIII)] \geq 20$, with $r_p = -0.28$, a correlation significant at the 3.4σ level. If this trend is maintained to higher redshifts, one may expect to observe a higher fraction of CIII] emitters in lower luminosity galaxies into the reionisation epoch than reported in Sect.5.

The SFR is also decreasing with increasing $EW(CIII)]$ ($r_p=0.3$, significant at 3.6σ), with a decrease of $\sim 20\%$ for emitters with $EW(CIII)] \geq 20$ compared to $5 < EW(CIII)] < 20$. With $EW(CIII)]$ dependent on the ionizing field, and the strongest CIII] emitters partially powered by AGN (Nakajima et al. 2017), this relation may be due to the quenching of star-formation. This is discussed in Sect.6.3.

There is a weak trend for the strongest CIII] emitters to have higher stellar masses than the weaker emitters, but this is not significant ($r_p = 0.08$, 0.6σ). The trend in SFR and M_{star} combine for a weak dependency of $SSFR$ with $EW(CIII)]$ ($r_p = -0.31$, 3.3σ). There is no apparent trend with $EW(CIII)]$ of the dust extinction from the $E(B-V)$ computed from SED fitting.

A visual morphological classification is performed on each of the CIII] samples (Tab.1), using the HST F814W images available in the COSMOS and ECDFS fields (for details on the imaging data on the VUDS sample, see Ribeiro et al. 2016b). The very strong CIII] emitters have a morphology dominated by compact galaxies ($r_{100} < 1$ kpc, see Ribeiro et al. 2016b) and galaxy pairs with separation less than 20 kpc (see Ribeiro et al.

Table 1. Visual classification of CIII] emitters morphology

Sample	Compact $r_T < 1\text{kpc}^1$	Pairs $r_p < 20\text{kpc}^2$	Clumpy & Extended
$0 < EW(CIII)] < 10\text{\AA}$	6%	40%	54%
$10 < EW(CIII)] < 20\text{\AA}$	39%	39%	22%
$EW(CIII)] > 20\text{\AA}$	25%	44%	31%

¹ Total radius (Ribeiro et al. 2016b)

² Transverse pair separation

2016a). The population of strong CIII] emitters shows a high fraction of compact galaxies, with an equal fraction of pairs. For the medium and weak emitters, the fraction of compact galaxies is low, the pair fraction remains similar to the other CIII] samples, but clumpy galaxies and those extended and symmetric dominate. It therefore appears that CIII] is preferentially emitted in compact and interacting systems, as already pointed out in the smaller VUDS sub-sample of Amorín et al. (2017). This is further supported by the distribution of sizes as a function of $EW(CIII)]$ presented in Fig.9, with sizes clearly decreasing with increasing $EW(CIII)]$ (with $r_p=-0.44$, a correlation significant at the 5.5σ level).

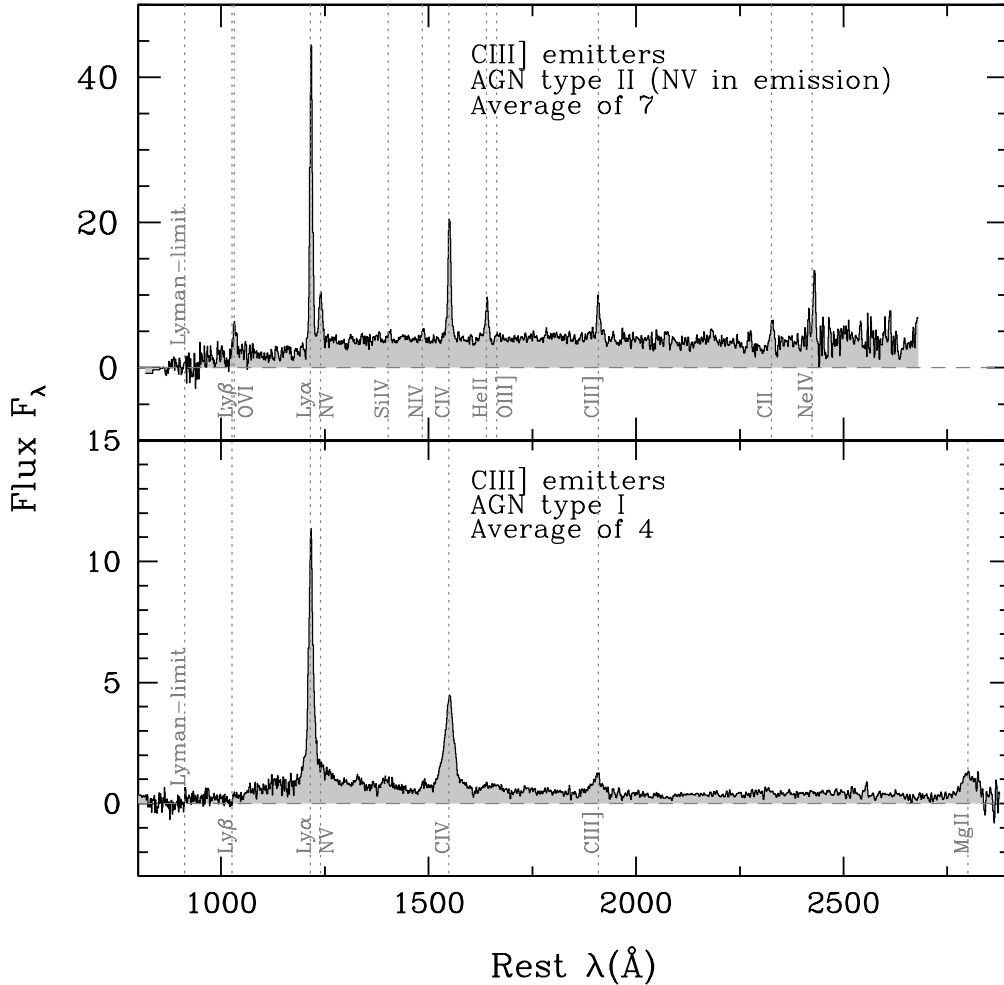


Fig. 6. Composite spectrum of 4 type I broad line AGN (bottom panel), and 7 candidate type II narrow line AGN identified from their NV- λ 1240 emission (top panel). See text for details on how these AGN are selected.

6.2. Outflow velocities

The velocity of ISM lines compared to the systemic velocity is presented in Fig.10 as measured from the stacked CIII] spectra, and the median velocity derived from the individual line measurements is presented in Fig.11. We set the systemic velocity on the CIII] line, and verified that this agrees with photospheric absorption lines CIII]- λ 1176 and SiV- λ 1501, as well as with HeII- λ 1640 emission (see Talia et al. 2017). To measure the velocity of the ISM we use the ISM absorption lines in Table 2 of Talia et al. (2017), except the FeII- λ 1608 line which is measured to be compatible for being at rest and may be contaminated by a blend of absorption features (FeIII, AlIII, NII) as pointed out by Talia et al. (2017). We also exclude the CIV- λ 1549 line, which is a combination of emission and absorption. For the whole SFG population at $2 < z < 3$ and $3 < z < 4$ and the CIII] emitters with $5 < EW(CIII)] < 10 \text{ \AA}$ we detect and use the above lines to compute the median velocity difference $\Delta V = \delta\lambda/\lambda \times c$. For $5 < EW(CIII)] < 10 \text{ \AA}$ emitters we do not use SiV- λ 1402.77 and AlIII - λ 1854.72, 1862.79 only weakly detected. For $EW(CIII)] > 20$ we use SiII- λ 1260, SiIV- λ 1393.76, 1402.77, SiII- λ 1526.71, and AlIII- λ 1854.72, 1862.79, with the other lines not detected in the stack of this smaller sample. At

the spectral resolution used for the VUDS sample (Sect. 2), the instrumental resolution is $\sim 1000 \text{ km/s}$, allowing for an accuracy in relative velocity measurements of $\sim 250 \text{ km/s}$ (Le Fèvre et al. 2015), and when all ISM lines are well detected as in the whole SFG samples at $2 < z < 3$ and $3 < z < 4$, the velocity dispersion of line velocity measurements is $\sigma_V(ISM) \sim 40 - 50 \text{ km/s}$.

The resulting relative velocity measurements are quite striking (Fig.11): we find low velocity outflows with 50 to 150 km/s for the whole SFG populations at $2 < z < 3$ and $3 < z < 4$ and medium CIII] emitters, while the outflow velocity increases to $445 \pm 110 \text{ km/s}$ for the strong $10 < EW(CIII)] < 20$ emitters, and reaches $1014 \pm 205 \text{ km/s}$ for the very strong emitters with $EW(CIII)] > 20$, well beyond the escape velocity of such galaxies (Cimatti et al. 2013), and comparable to what is observed in SFGs with AGN at $z \sim 1-2$ (e.g. Genzel et al. 2014). As star formation does not seem to be capable to produce outflow velocities beyond $\sim 600 \text{ km/s}$ even for strong starbursts with maximally efficient winds (Thacker et al. 2006), we conclude that the outflows reported here for the stronger CIII] emitters are produced by an AGN. This is further discussed in the following sections.

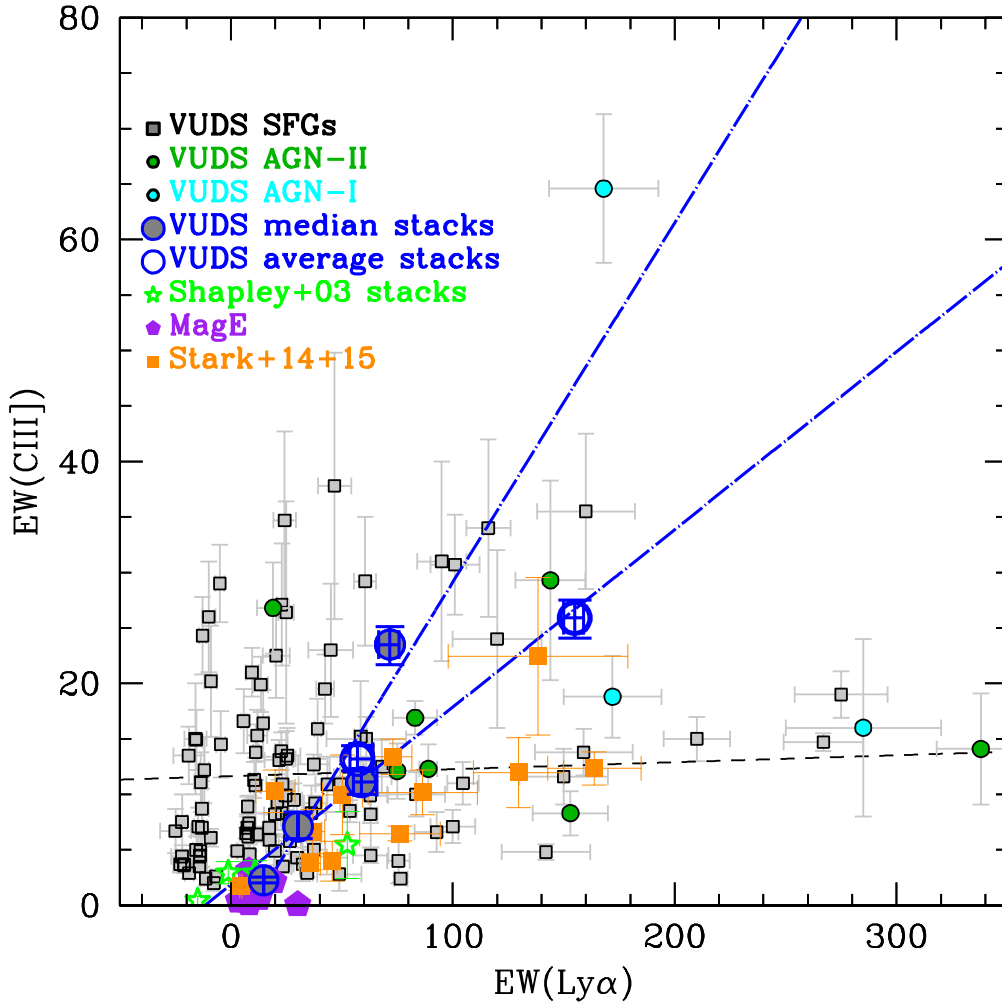


Fig. 7. Rest-frame equivalent width of CIII]- λ 1908Å $EW(CIII])$ as a function of $EW(Ly\alpha)$. The least square fit to the individual data points (black squares) is represented by the black dashed line. The individual galaxies show only a weak correlation, significant at about the 3σ level, with a large dispersion, with a large dispersion. Galaxies with strong $Ly\alpha$ and weak CIII] are observed, as well as galaxies with strong CIII] and $Ly\alpha$ in absorption. The $EW(CIII])$ versus $EW(Ly\alpha)$ points for the median-stacked spectra of the different categories defined in Sect.3.1 are indicated as blue circles filled in gray, while values for the average stacks in Tab.2 are indicated as the open blue circles. The correlation between $EW(CIII])$ and $EW(Ly\alpha)$ appears as very strong ($r_p = 0.99$, $r_s = 1$), hiding the wide range of properties of CIII] vs. $Ly\alpha$. As a comparison with the literature, we plot the observed values from the different $Ly\alpha$ samples of Shapley et al. (2003) (green stars, average for $Ly\alpha$ samples), Rigby et al. (2015) (purple diamonds), and Stark et al. (2014, 2015) (orange squares).

6.3. CIII] emitters in the SFR vs. M_{star} plane

The position of CIII] emitters with respect to the main sequence (MS) of star-forming galaxies in the stellar mass vs. SFR plane is presented in Fig.12. The strong and very strong emitters show a trend of being located below the main sequence (MS) observed in the same redshift range (Tasca et al. 2015). This is particularly evident for the very strong emitters with $EW(CIII]) > 20$, which are mostly below the MS. For this population it is quite striking to observe galaxies with low or even very low SFR, but with very strong CIII] emission. In Fig.13 we present the distribution of the difference between the SFR of galaxies and the main sequence identified in Fig.12. The mean SFR difference increases from $d_{MS}(SFR) = +0.14 \pm 0.03$ (dex, above the MS) for emitters with $0 < EW(CIII]) < 10\text{\AA}$, to $d_{MS}(SFR) = -0.10 \pm 0.08$ for $10 < EW(CIII]) < 20\text{\AA}$, to $d_{MS}(SFR) = -0.27 \pm 0.07$ (below the MS) for $EW(CIII]) > 20\text{\AA}$. The total shift in SFR of

$d_{MS}(SFR) = -0.41$ dex between the weak CIII] emitters and the very strong emitters is significant at more than a 5σ level.

The star formation of the weaker CIII] emitters appears to be higher than for the bulk of the SFGs. While the whole SFG population has a median $EW(CIII]) \sim 2\text{\AA}$ (Tab.2), the population of weak and medium emitters have $EW(CIII]) = 3.4\text{\AA}$ and 8.0\AA , respectively. Producing $3 < EW(CIII]) < 10\text{\AA}$ in the absence of an AGN requires enhanced star formation consistent with this population being above the MS (Nakajima et al. 2017).

The distance to the MS of the strong and very strong CIII] emitters is more puzzling, as the distance to the MS of these populations is increasingly below the MS, with a star formation rate about half that on the MS. A possible interpretation is that the star formation for a fraction of the strong emitters and a majority of the very strong emitters is subject to quenching of star formation. Some of the very strong emitters are more than a fac-

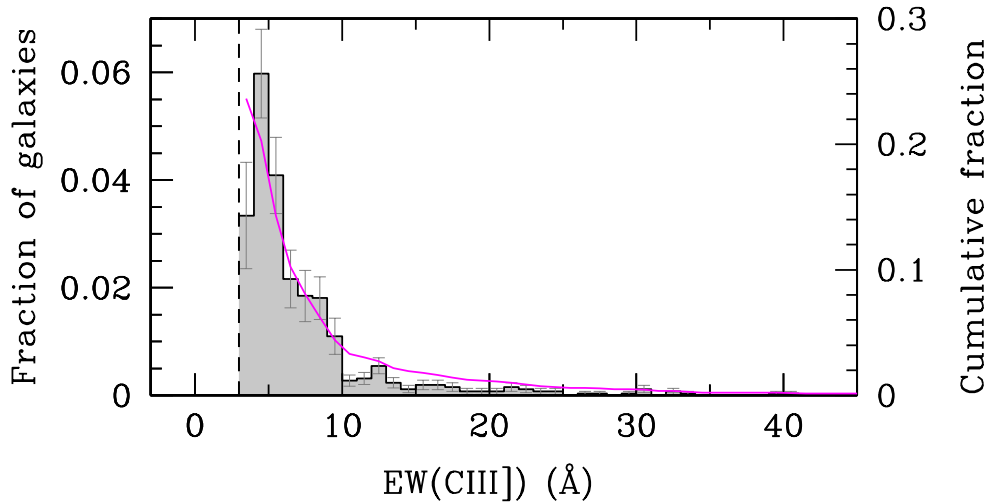


Fig. 8. Distribution of CIII]- λ 1908 equivalent width $EW(CIII])$ in the UV-selected star-forming population at $2 < z < 3.8$. The shaded histogram shows the fraction of galaxies with a given $EW(CIII])$ in bins of $\delta EW = 1 \text{ \AA}$ (left Y-axis), with Poisson uncertainties from the population statistics indicated as error bars. The cumulative fraction of galaxies with $EW(CIII])$ above a given $EW(CIII])$ limit is drawn as the continuous magenta line (values on the right Y-axis), relative to the total population of SFGs at that redshift. About 24% of SFGs with $2 < z < 3.8$ present CIII]- λ 1908Å emission with $EW(CIII]) \geq 3 \text{ \AA}$.

tor of 10 below the MS, which means that the quenching must be very effective, while, at the same time, maintaining a very strong ionizing field needed to produce $EW(CIII])$ in excess of 20 \AA .

We further investigate the properties of the CIII] emitters looking at the age distribution of the different categories, as presented in Fig.14, with ages computed in Thomas et al. (2017) from the joint fitting of VUDS spectra and rest-UV and optical photometry. We use as an age definition the time since the onset of the last star formation event which dominate the star formation history, as modeled by a delayed exponential (see Thomas et al. 2017). The median age of the galaxies is about the same for the weak and medium emitters, with 0.29 ± 0.07 and 0.30 ± 0.05 Gyr respectively, it increases to 0.46 ± 0.09 Gyr for the strong emitters, and reaches up to 0.82 ± 0.13 Gyr for the very strong emitters. This relative age difference does not qualitatively change when using other age definitions like the mass-weighted age.

As pointed out in Sect.2 as AGN might not dominate the age sensitive regions of the SED, the presence of AGN is not expected to significantly alter the stellar mass or SFR measurements obtained from SED fitting (see e.g. Bongiorno et al. 2012) and the results presented here are thus qualitatively expected to hold. However, more sophisticated SED modeling will be in order when higher signal to noise data will become available to separate AGN from stellar populations.

7. Evidence for AGN quenching star-formation

Several feedback-related quenching processes have been proposed, including AGN feedback, stellar wind feedback from supernovae and massive stars, or environmental quenching (e.g. Croton et al. 2006; Hopkins et al. 2008; Gabor et al. 2010, 2011). Various pieces of evidence presented in this paper converge to point out that the dominant process producing the ob-

served quenching of star formation in strong CIII] emitters is AGN related.

Starting from the perspective of analyzing the population of CIII] emitters, we have uncovered several important and related observed properties. We find a population of galaxies with high $EW(CIII])$, reaching in excess of 20 \AA (Sect.3.1). These strong emitters require a strong ionizing field beyond what stellar populations can produce, but rather at a level to what can be produced by AGN (Nakajima et al. 2017). Emission line properties indicate that a fraction of these galaxies must host an AGN as discussed in Sect.3.2, and as extensively studied with line ratio diagnostics in Nakajima et al. (2017). Nakajima et al. (2017) use line diagnostics defined from a large grid of photoionization models including stellar populations and AGN to find that about a third of the strong and very strong emitters in VUDS require the presence of an AGN to explain the high $EW(CIII])$ and the position of individual emitters in line ratio diagnostic diagrams. The strongest emitters present strong outflows with velocity above 800 km/s beyond what stellar winds can produce, and rather comparable to that of AGN (Talia et al. 2017). In addition, we find that the strongest CIII] emitters appear below the main sequence, with SFR lower by about 0.4 dex for the stronger emitters compared to the weak emitters, and mean ages almost three times older than the SFG population (Sect.6.3). The analysis of stacked X-ray imaging presented in Sect.3.2 further indicates a marginal detection (2σ) for the strongest CIII] emitters consistent with the presence of a low luminosity AGN with $L_X(2-10 \text{ keV}) < 3 \times 10^{42} \text{ erg/s}$ hosted by those galaxies.

These observed properties all converge to favor AGN feedback as the main physical process capable of quenching the star formation in the strong and very strong CIII] emitters. In an empirical scenario the strong ionizing field is produced by AGN hosted in the galaxies observed as CIII] emitters. The jets and winds associated to the AGN would produce strong feedback,

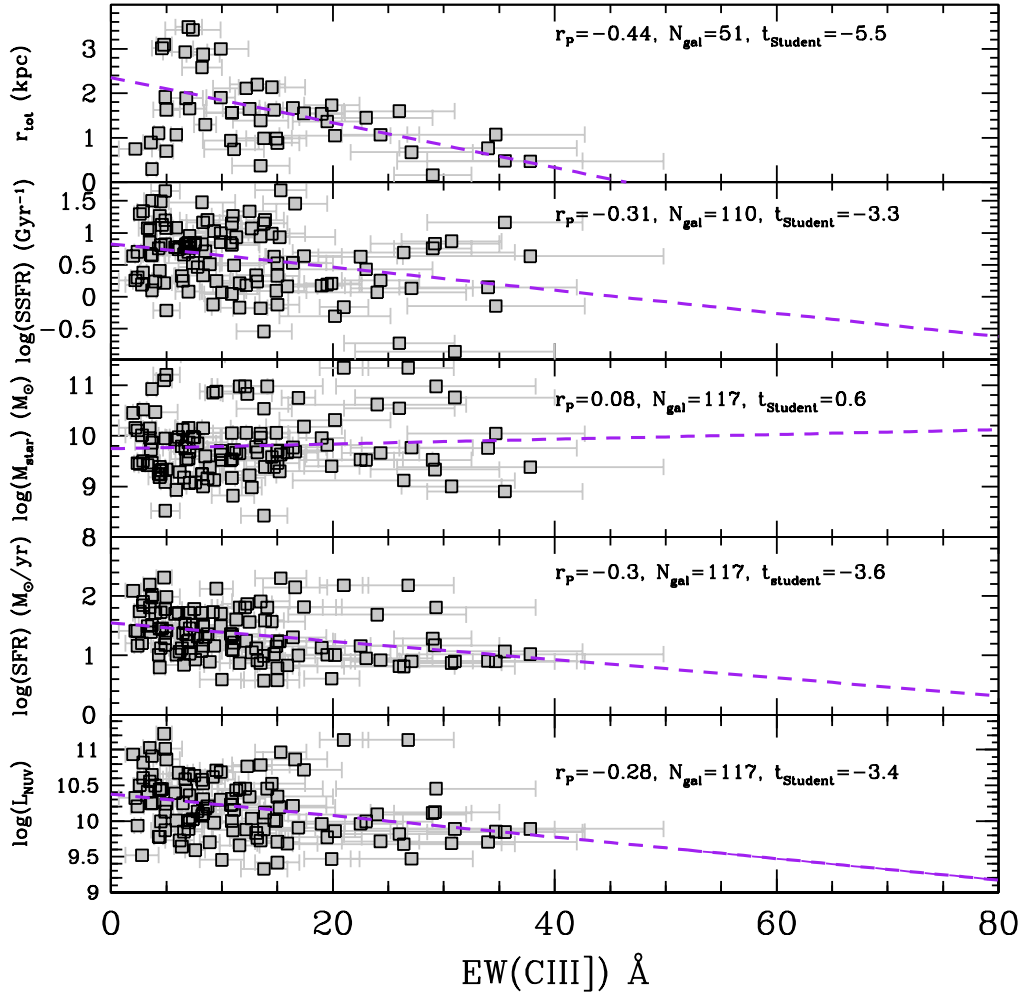


Fig. 9. Properties of CIII] emitters, from bottom to top: L_{NUV} , SFR, M_{star} , SSFR, and total size properties of CIII] emitters as a function of $EW(CIII)]$. A least square fit to the data is shown as the purple dashed lines, and the Pearson correlation coefficient r_p , number of objects, and the significance of the correlation (Student t-test), are indicated on the upper right corner of each panel. Note that the r_{tot} measurements are limited to the COSMOS and ECDFS fields where HST imaging is available (Ribeiro et al. 2016b).

depositing energy in the ISM, gradually removing the gas supply and effectively quenching star formation, driving those galaxies below the MS. The large age difference of up to a factor of three observed between the CIII] emitters and main sequence galaxies may then indicate that the AGN feedback is taking at most a few hundred million years to operate. We therefore infer that part of the star-forming population is undergoing AGN feedback with the quenching of star formation, at any given time 10.5 to 12.2 Gyr after the Big Bang.

With one third of the strong and very strong CIII] emitters in the SFG sample which must host an AGN (Nakajima et al. 2017), AGN feedback then concerns about one third of the 4% of the SFG population that we identify with $EW(CIII)] > 10\text{\AA}$. If the duration of AGN activity at an energy level required to produce galaxy-wide quenching star-formation is less than the cosmic time covered by our observations, the fraction of the SFG population experiencing AGN feedback and quenching could be significantly higher. We estimate the quenching timescale assuming that SFGs subject to AGN feedback will then transform into the quiescent galaxies observed at $z \sim 2$. The volume density of quiescent galaxies with a stellar mass $M_{star} > 10^{10}M_{\odot}$

at $z \sim 2$ is reported to be $\sim 3 \times 10^{-3}$ gal/Mpc³ (Brammer et al. 2011; Ilbert et al. 2013; Barro et al. 2013). From the analysis in this paper, one third of 4% of SFGs above this mass translates into 3.3×10^{-4} gal/Mpc³. For SFGs at a redshift $z \sim 3$ to transform into the right number of quiescent galaxies over a cosmic time of 1.1 Gyr to $z \sim 2$ then requires a quenching timescale $T_{quench} = (3.3 \times 10^{-4} / 3 \times 10^{-3}) \times 1.1$ Gyr, or about 0.35 Gyr, with a range 0.25 – 0.47 Gyr given uncertainties on the AGN fraction. The effective timescale for star-formation quenching from AGN feedback is currently highly uncertain from one hundred million years up to several hundred million years (, see e.g. Cattaneo et al. 2009; Kaviraj et al. 2011; Schawinski et al. 2014). Our results therefore seem to favor a long quenching timescale, as timescales much shorter than 0.35 Gyr would seem to overproduce quiescent galaxies by $z \sim 2$. However, these numbers are indicative and will need to be refined with improved statistics on both the fraction of SFGs subject to AGN feedback, as well as on galaxies truly quiescent by $z \sim 2$. Those numbers could also need to be adjusted if AGN feedback is only one of several ways to quench star formation for galaxies with $M_{star} > 10^{10}M_{\odot}$.

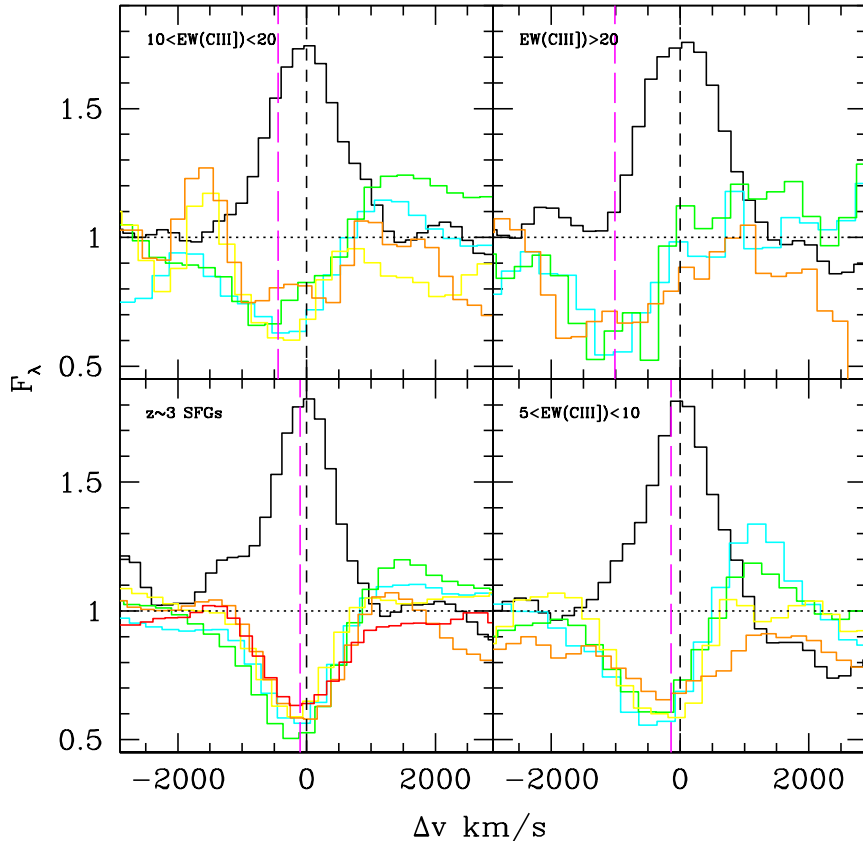


Fig. 10. Relative velocity of the main ISM absorption lines with respect to CIII]- λ 1908Å taken at systemic velocity, for the SFG population and samples with increasing EW(CIII)]. CIII] is in black, and depending on the sample SiII- λ 1260 is drawn in cyan, SiII- λ 1303 in green, CII- λ 1334 in yellow, 1526 in orange, and 1670 in red.

Our results offer additional evidence for the co-evolution of AGN and star-formation at $z \sim 2 - 4$. Star formation is observed to be present coevally with AGN activity (e.g. Fabian 2012; Cimatti et al. 2013; Karman et al. 2014; Lemaux et al. 2013; Ishibashi & Fabian 2016), and this is what we are witnessing in the strong CIII] emitters population.

8. Discussion and summary

In this paper we present a statistical analysis of the properties of CIII]- λ 1908 emitters with two aims: investigate the prevalence of CIII] emission in the star-forming galaxy population, and characterize the properties of the population of CIII] emitters using CIII] as a diagnostic tool, using measurements from the large sample of 3899 galaxies with $2 < z < 3.8$ in the VIMOS Ultra-Deep Survey (VUDS), .

The VUDS sample is selected from UV rest-frame luminosity ($i_{AB} \leq 25$) and provides a large unbiased sample of UV-selected star-forming galaxies in a large volume minimizing cosmic variance (Le Fèvre et al. 2015), ideally suited to search for CIII] emitters, explore their properties and derive the frequency of appearance of this emission line. Spectral line measurements including lines from Ly β up to CIII] is made possible from the deep VIMOS spectra. In addition, spectral model fitting performed simultaneously on spectra and multi-band photometry (Thomas et al. 2017) provides physical parameters including

stellar mass, SFR, age, and dust extinction, which are used to characterize the population of CIII] emitters.

We split our sample in four categories of CIII] emitters spanning a range from weak emitters $0 < EW(CIII)]_{rest} < 5 \text{ \AA}$ to very strong emitters with observed EW(CIII)] up to $\approx 40 \text{ \AA}$ for narrow line emission spectra. Individual spectra are stacked to produce average spectral properties for each category (Figures 4 and 5). We find that, as EW(CIII)] increases, emission lines requiring higher ionizing potential appear, with the strongest emitters showing NV- λ 1240, SiII- λ 1309, SiIV- λ 1403, NIV]- λ 1485, CIV- λ 1549, HeII- λ 1640, OIII]- λ 1663, NIII]- λ 1750, SiIII]- λ 1888 (Fig. 5).

We find a correlation between Ly α emission and CIII] emission (Figure 7), but with a large dispersion as we find strong CIII] emitters with Ly α in absorption, or strong Ly α emission and no or weak CIII]. We explore the properties of the CIII] population and find that EW(CIII)] weakly increases with near-UV luminosity L_{NUV} , and that the total size of galaxies gets smaller as EW(CIII)] increases (Fig.9).

From the complete VUDS sample we compute the distribution of EW(CIII)] (Fig.8) and find that about 24% of the population shows some sign of CIII] emission. A first visual impression was already given in the Figure 10 of Le Fèvre et al. (2015), as CIII] can be followed clearly from the 2D spectra image of the whole VUDS sample. We quantify this statement, finding that 20% of the population shows weak emission with $3 < EW(CIII)] < 10 \text{ \AA}$, 4% has $EW(CIII)] > 10 \text{ \AA}$, and 1.2%

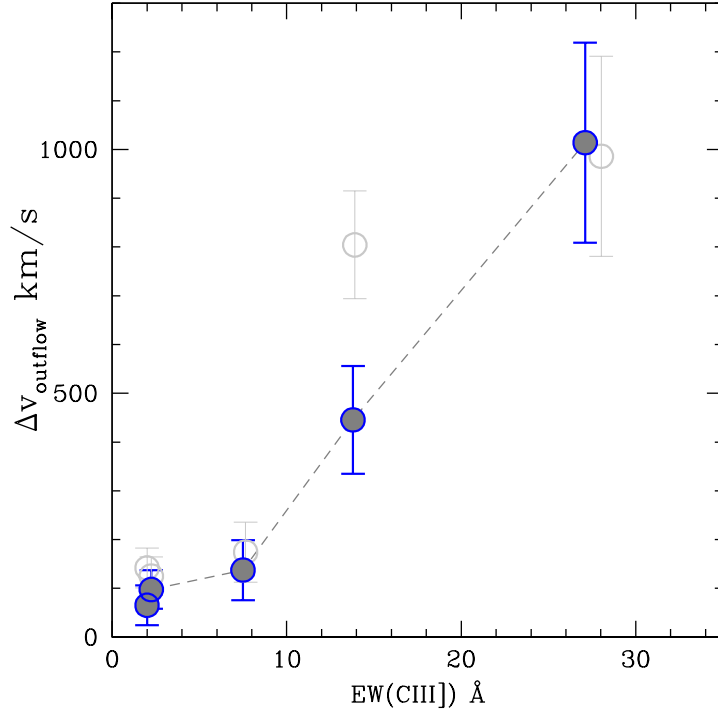


Fig. 11. Outflow velocity of ISM lines as a function of $EW(CIII])$ (filled symbols: velocity from the median values of the ISM lines, open symbols: mean values)

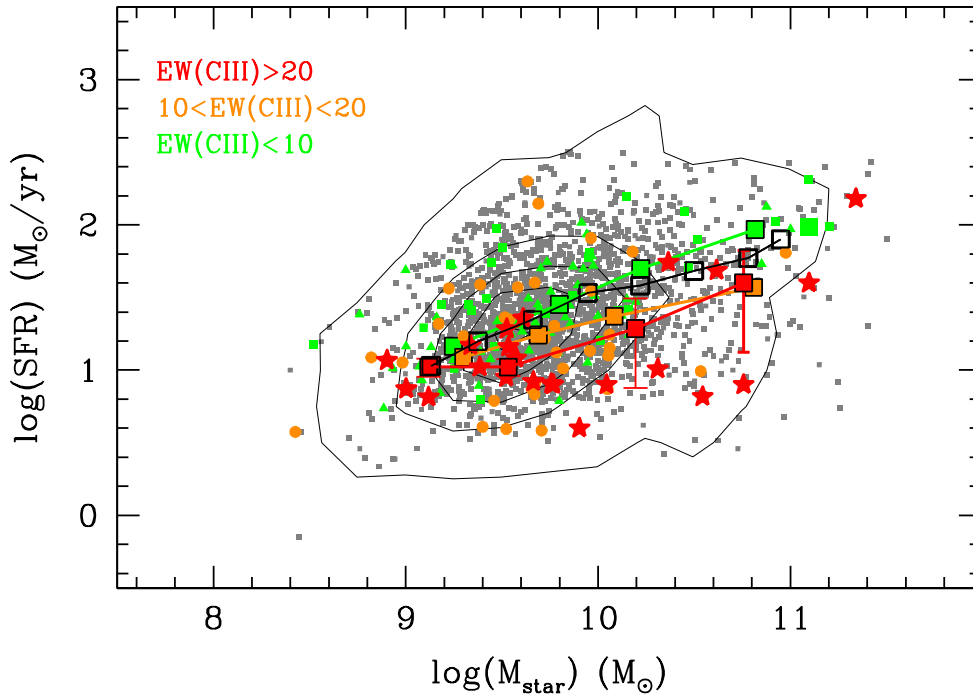


Fig. 12. Distribution of CIII] emitters with different $EW(CIII])$ in the M_{star} -SFR plane. The CIII] emitters with different EW are identified by the different colored symbols. The parent sample of star-forming galaxies at redshifts $2 < z < 3.8$ in VUDS is identified as grey symbols with their distribution identified by the contours, and the main sequence of VUDS galaxies at $z \sim 3$ is indicated by black open squares connected by a thick line. We note that both the strong and very strong CIII] emitters are on average below the MS, with median values identified by the connected orange and red squares, respectively. The lower SFR of these strong CIII] emitters compared to the MS is possibly resulting from a strong star formation quenching produced by AGN feedback in the host star-forming galaxies.

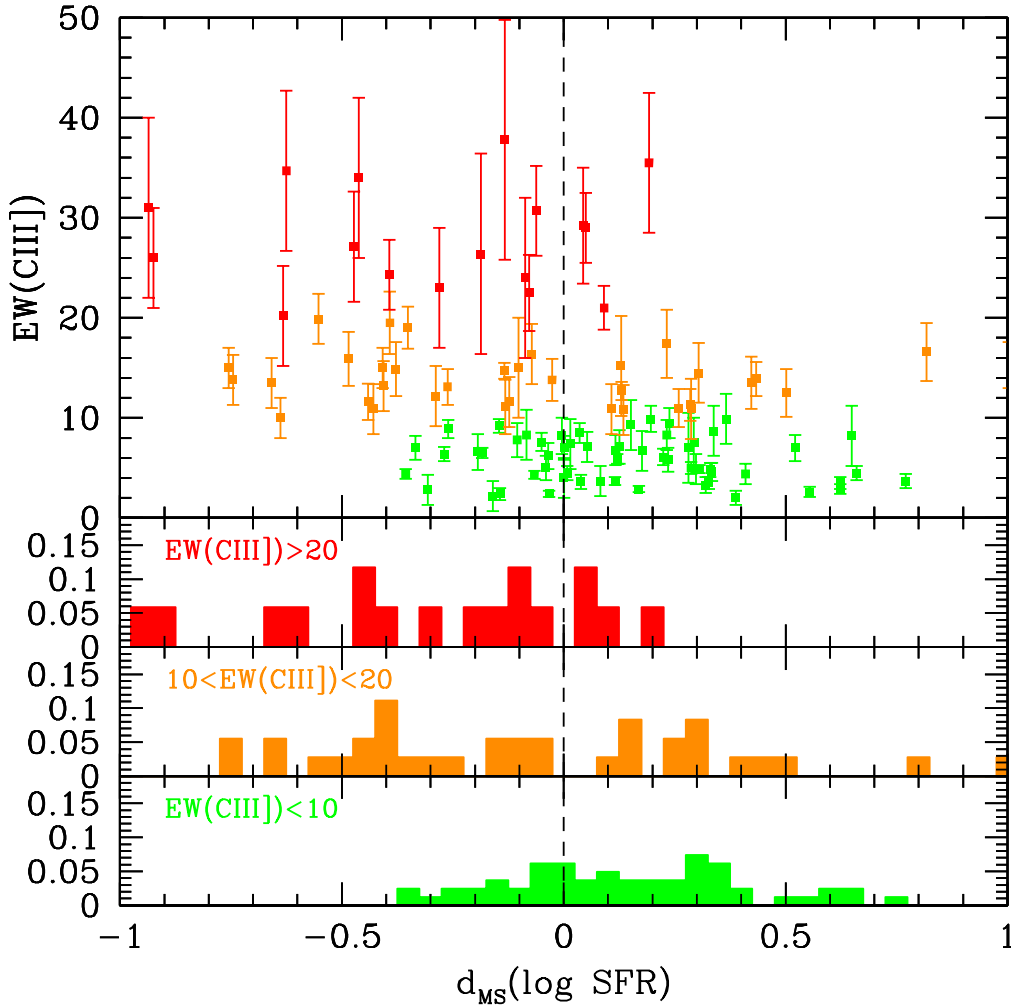


Fig. 13. (*bottom three panels*) Distribution of distances in SFR from the main sequence for CIII] emitters with increasing $EW(CIII)]$; (*top panel*) Distance to the main sequence for individual CIII] emitters. As $EW(CIII)]$ increases the distance to the main sequence increases.

presents very strong emission with $EW(CIII)] > 20\text{\AA}$. We find that LAE have a 42% chance to show CIII] in emission with $EW(CIII)] > 3\text{\AA}$.

While the presence of CIII] emission therefore appears rather frequent, we note that the vast majority of CIII] emitters are weak emitters making this line difficult to identify, except for the $\sim 4\%$ of the population with $EW(CIII)] > 10\text{\AA}$. One therefore cannot expect to rely on CIII] emission alone as a means to measure the spectroscopic redshifts of galaxies in a complete sample of SFGs. Redshift measurements of UV-rest spectra without Ly α emission will still need to rely on a combination of the most prominent spectral features. Typically, besides CIII], lines like CIV, HeII, the continuum break at and below Ly α , and hard-to-detect absorption features can jointly serve to eliminate degenerate redshift solutions.

The fraction of strong CIII] emitters is expected to increase at higher redshifts towards the epoch of HI reionization (EoR) at $z > 6$, only in the presence of a stronger ionizing field than observed in our sample at $2 < z < 3.8$, together with very low metallicity. Such conditions may exist in the lower luminosity galaxies in our sample (Sect.6.1) and such galaxies may be prevalent in the EoR. Some analogs to those expected in the EoR

have been discussed in Amorín et al. (2017). It is well possible that as the population of forming galaxies gets younger, with lower stellar mass, and lower metallicity, the fraction of objects with strong CIII] emission in the EoR would be higher than in our sample at $z \sim 3$. This may be the case for the very first generation of stars in the first galaxies (Nakajima et al. 2017). Exactly how this fraction of strong emitters will increase at higher redshifts remains to be investigated.

The main result from this paper is a coherent set of observational evidence pointing to AGN feedback acting on the population of strong CIII] emitters. Upon examination of spectral features, we identify four galaxies with broad emission lines, their quasar-like spectra clearly powered by strong AGN. We identify 7 objects with NV- λ 1240 narrow emission line $EW(NV)] > 10\text{\AA}$ recognized as a potential tracer of AGN activity. The most striking observational results include the clear evidence for strong outflows up to ~ 1000 km/s for the strongest CIII] emitters, and increasingly lower SFR in the SFR- M_{star} plane as $EW(CIII)]$ increases. Such strong outflows require energy levels beyond what stellar winds are capable to produce on a galaxy scale but are consistent with being powered by AGN (e.g. Harrison et al. 2012; Cimatti et al. 2013; Förster Schreiber et al.

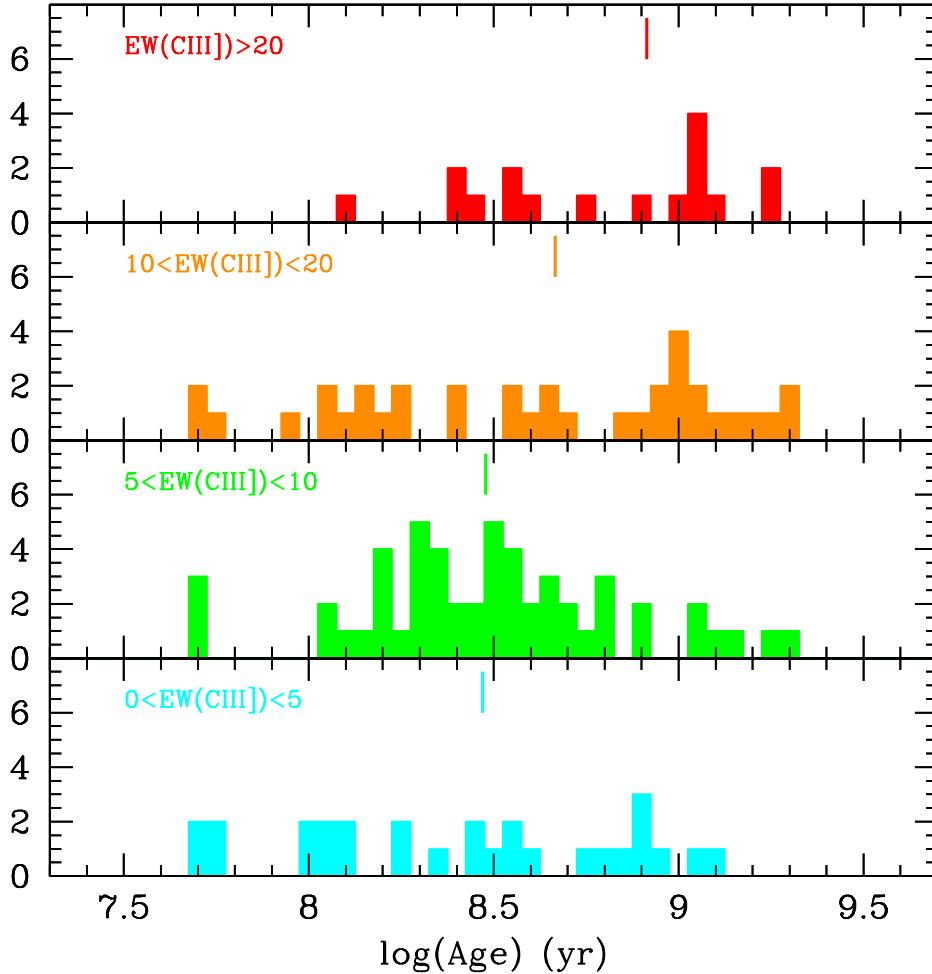


Fig. 14. Age distribution of CIII] emitters with different EW(CIII]). The median age of each population is identified by the vertical lines color as for their respective sub-samples. The strength of the CIII] emission increases with the mean age.

2014; Brusa et al. 2015). The distribution of CIII] emitters in the stellar mass vs. SFR plane around the main sequence of star-forming galaxies is investigated in Fig.12. Our analysis shows that the strong and very strong emitters are on average below the MS indicating that the star formation is quenched in these galaxies, with the SFR decreasing when EW(CIII]) increases. From X-ray data stacking, we find a marginal 2σ detection consistent with low luminosity AGN with $L_X(2-10 \text{ keV}) \sim 42.9 \text{ erg/s}$ for the strong and very strong CIII] emitters, as observed on the faint end of the AGN luminosity function at these redshifts (Georgakakis et al. 2015).

The physical origin of CIII] emission in relation to the prevalent ionizing field is investigated in Nakajima et al. (2017). From the data presented here, Nakajima et al. (2017) derive various line ratio diagnostics on the basis of a large range of photoionizing models combining CIII]- λ 1908 with other emission lines like CIV- λ 1549, HeII- λ 1640, OIII]- λ 1664. It is found that the strong and very strong CIII] emitters must host an AGN in order to produce the large EW(CIII]) and observed line ratios. The spectral analysis in Nakajima et al. (2017) therefore reinforces our proposed scenario with strong AGN-driven quenching of star-formation. Without AGN, it seems unlikely to find conditions with the high star-formation activity necessary to produce

strong CIII] and the observed line ratios, while at the same time producing strong outflows and driving galaxies off the MS. We rather conclude that it is more realistic that AGN and star formation activity act together to produce the observed properties of CIII] emitters.

The signature of AGN have been previously reported in SFGs at and beyond the peak in SFRD (e.g. Cimatti et al. 2013; Genzel et al. 2014; Talia et al. 2012; Karman et al. 2014; Talia et al. 2017). The regulation of mass growth from the quenching of star-formation has been proposed to support an evolutionary path gradually transforming SFGs at the highest redshifts into quiescent galaxies observed at $z \sim 1 - 2$ (Barro et al. 2013), with AGN feedback identified from numerical simulations as the prime contender for the quenching of star formation (Hopkins et al. 2006, 2008). The results presented in this paper bring further evidence of the presence of AGN in SFGs at a key epoch of mass build-up in galaxies

The properties of CIII] emitters are consistent with an empirical scenario in which CIII] emitting galaxies with increasing EW host an increasingly larger fraction of AGN producing the strong ionizing field needed to ionize CIII] to the observed levels. Those AGN drive the strong observed outflows, and in the end quench star-formation in the host galaxies to pro-

duce the observed location of CIII] emitters in the $SFR-M_{star}$ plane. The age of the stellar populations of the stronger emitters is found to be about three times that of the weak emitters, at ~ 0.8 vs. 0.3 Gyr, respectively. This may be an indication that the strongest emitters were the first to experience AGN feedback and associated quenching. We find that quenching timescales of $\sim 0.25 - 0.5 \times 10^8$ years are required to transform SFGs with $M_{star} > 10^{10} M_{\odot}$ into the volume density of quiescent galaxies observed at $z \sim 2$ (Brammer et al. 2011; Ilbert et al. 2013; Barro et al. 2013).

We conclude that the co-evolution of stellar populations and AGN is a key ingredient to the star formation evolution and mass build-up in galaxies at these early times. Future experiments assembling larger datasets will be necessary to investigate whether the AGN feedback and quenching identified in the redshift range of this paper and beyond is mass-dependent.

The results presented here point to the need for large comprehensive spectroscopic surveys with the power to identify galaxy populations which may appear as rare but provide important clues on the first phases of galaxy assembly. Our study paves the way to a systematic use of spectral line properties and diagnostics from the UV to optical rest-frame for future investigations using next generation facilities like the James Webb Space Telescope and ELTs.

Acknowledgements. This work is supported by funding from the European Research Council Advanced Grant ERC-2010-AdG-268107-EARLY and by INAF Grants PRIN 2010, PRIN 2012 and PICS 2013. AC, OC, MT and VS acknowledge the grant MIUR PRIN 2015. This work is based on data products made available at the CESAM data center, Laboratoire d'Astrophysique de Marseille, France.

References

Alexandroff, R., Strauss, M. A., Greene, J. E., et al. 2013, *MNRAS*, 435, 3306
 Amorín, R., Fontana, A., Pérez-Montero, E., et al. 2017, *Nature Astronomy*, 1, 0052
 Assef, R. J., Kochanek, C. S., Brodwin, M., et al. 2010, *ApJ*, 713, 970
 Barro, G., Faber, S. M., Pérez-González, P. G., et al. 2013, *ApJ*, 765, 104
 Best, P. N., Röttgering, H. J. A., & Longair, M. S. 2000, *MNRAS*, 311, 23
 Bongiorno, A., Merloni, A., Brusa, M., et al. 2012, *MNRAS*, 427, 3103
 Bournaud, F., Chapon, D., Teysier, R., et al. 2011, *ApJ*, 730, 4
 Bouwens, R. J., Illingworth, G. D., Oesch, P. A., et al. 2015, *ApJ*, 803, 34
 Bradač, M., García-Appadoo, D., Huang, K.-H., et al. 2017, *ApJ*, 836, L2
 Brammer, G. B., Whitaker, K. E., van Dokkum, P. G., et al. 2011, *ApJ*, 739, 24
 Brusa, M., Bongiorno, A., Cresci, G., et al. 2015, *MNRAS*, 446, 2394
 Bundy, K., Georgakakis, A., Nandra, K., et al. 2008, *ApJ*, 681, 931
 Capak, P. L., Carilli, C., Jones, G., et al. 2015, *Nature*, 522, 455
 Carilli, C. L. & Walter, F. 2013, *ARA&A*, 51, 105
 Cassata, P., Le Fèvre, O., Charlot, S., et al. 2013, *A&A*, 556, A68
 Cassata, P., Tasca, L. A. M., Le Fèvre, O., et al. 2015, *A&A*, 573, A24
 Cattaneo, A., Faber, S. M., Binney, J., et al. 2009, *Nature*, 460, 213
 Chiappetti, L., Clerc, N., Pacaud, F., et al. 2013, *MNRAS*, 429, 1652
 Cimatti, A., Brusa, M., Talia, M., et al. 2013, *ApJ*, 779, L13
 Civano, F., Elvis, M., Brusa, M., et al. 2012, *ApJS*, 201, 30
 Civano, F., Marchesi, S., Comastri, A., et al. 2016, *ApJ*, 819, 62
 Croton, D. J., Springel, V., White, S. D. M., et al. 2006, *MNRAS*, 365, 11
 De Barros, S., Pentericci, L., Vanzella, E., et al. 2017, *ArXiv e-prints*
 Du, X., Shapley, A. E., Martin, C. L., & Coil, A. L. 2016, *ArXiv e-prints*
 Dubois, Y., Gavazzi, R., Peirani, S., & Silk, J. 2013, *MNRAS*, 433, 3297
 Erb, D. K., Pettini, M., Shapley, A. E., et al. 2010, *ApJ*, 719, 1168
 Fabian, A. C. 2012, *ARA&A*, 50, 455
 Förster Schreiber, N. M., Genzel, R., Newman, S. F., et al. 2014, *ApJ*, 787, 38
 Gabor, J. M., Davé, R., Finlator, K., & Oppenheimer, B. D. 2010, *MNRAS*, 407, 749
 Gabor, J. M., Davé, R., Oppenheimer, B. D., & Finlator, K. 2011, *MNRAS*, 417, 2676
 Garilli, B., Fumana, M., Franzetti, P., et al. 2010, *PASP*, 122, 827
 Genzel, R., Förster Schreiber, N. M., Rosario, D., et al. 2014, *ApJ*, 796, 7
 Georgakakis, A., Aird, J., Buchner, J., et al. 2015, *MNRAS*, 453, 1946
 Guita, L., Talia, M., Pentericci, L., et al. 2017, *A&A*, 606, A19

Hainline, K. N., Shapley, A. E., Greene, J. E., & Steidel, C. C. 2011, *ApJ*, 733, 31
 Hainline, K. N., Shapley, A. E., Greene, J. E., et al. 2012, *ApJ*, 760, 74
 Hensch, R. W. 2003, *A&A*, 407, 1157
 Harrison, C. M., Alexander, D. M., Swinbank, A. M., et al. 2012, *MNRAS*, 426, 1073
 Hathi, N. P., Le Fèvre, O., Ilbert, O., et al. 2016, *A&A*, 588, A26
 Heckman, T. M., Borthakur, S., Overzier, R., et al. 2011, *ApJ*, 730, 5
 Hoag, A., Bradac, M., Trenti, M., et al. 2017, *Nature Astronomy*, 1, 0091
 Hopkins, P. F., Hernquist, L., Cox, T. J., et al. 2006, *ApJS*, 163, 1
 Hopkins, P. F., Hernquist, L., Cox, T. J., & Kereš, D. 2008, *ApJS*, 175, 356
 Ilbert, O., McCracken, H. J., Le Fèvre, O., et al. 2013, *A&A*, 556, A55
 Ishibashi, W. & Fabian, A. C. 2016, *MNRAS*, 463, 1291
 Karman, W., Caputi, K. I., Trager, S. C., Almaini, O., & Cirasuolo, M. 2014, *A&A*, 565, A5
 Kaviraj, S., Schawinski, K., Silk, J., & Shabala, S. S. 2011, *MNRAS*, 415, 3798
 Kehrig, C., Vilchez, J. M., Pérez-Montero, E., et al. 2015, *ApJ*, 801, L28
 Le Fèvre, O., Saisse, M., Mancini, D., et al. 2003, in *Society of Photo-Optical Instrumentation Engineers (SPIE) Conference Series*, Vol. 4841, Instrument Design and Performance for Optical/Infrared Ground-based Telescopes, ed. M. Iye & A. F. M. Moorwood, 1670–1681
 Le Fèvre, O., Tasca, L. A. M., Cassata, P., et al. 2015, *A&A*, 576, A79
 Lemaux, B. C., Le Floch, E., Le Fèvre, O., et al. 2013, *ArXiv e-prints*
 Lemaux, B. C., Lubin, L. M., Shapley, A., et al. 2010, *ApJ*, 716, 970
 Luo, B., Brandt, W. N., Xue, Y. Q., et al. 2017, *ApJS*, 228, 2
 Marchesi, S., Civano, F., Elvis, M., et al. 2016, *ApJ*, 817, 34
 Matsuoka, K., Nagao, T., Maiolino, R., Marconi, A., & Taniguchi, Y. 2009, *A&A*, 503, 721
 Moster, B. P., Somerville, R. S., Newman, J. A., & Rix, H.-W. 2011, *ApJ*, 731, 113
 Nakajima, K., Schaerer, D., Le Fèvre, O., et al. 2017, *ArXiv e-prints*
 Oesch, P. A., Brammer, G., van Dokkum, P. G., et al. 2016, *ApJ*, 819, 129
 Ouchi, M., Shimasaku, K., Akiyama, M., et al. 2008, *ApJS*, 176, 301
 Pentericci, L., Carniani, S., Castellano, M., et al. 2016, *ApJ*, 829, L11
 Pentericci, L., Fontana, A., Vanzella, E., et al. 2011, *ApJ*, 743, 132
 Pentericci, L., Vanzella, E., Fontana, A., et al. 2014, *ApJ*, 793, 113
 Ribeiro, B., Le Fèvre, O., Cassata, P., et al. 2016a, *ArXiv e-prints*
 Ribeiro, B., Le Fèvre, O., Tasca, L. A. M., et al. 2016b, *A&A*, 593, A22
 Rigby, J. R., Bayliss, M. B., Gladders, M. D., et al. 2015, *ApJ*, 814, L6
 Robertson, B. E., Ellis, R. S., Furlanetto, S. R., & Dunlop, J. S. 2015, *ApJ*, 802, L19
 Schaerer, D. 2003, *A&A*, 397, 527
 Schawinski, K., Urry, C. M., Simmons, B. D., et al. 2014, *MNRAS*, 440, 889
 Schmidt, K. B., Huang, K.-H., Treu, T., et al. 2017, *ApJ*, 839, 17
 Schmidt, K. B., Treu, T., Bradač, M., et al. 2016, *ApJ*, 818, 38
 Scodreggio, M., Franzetti, P., Garilli, B., et al. 2005, *PASP*, 117, 1284
 Shapley, A. E., Steidel, C. C., Pettini, M., & Adelberger, K. L. 2003, *ApJ*, 588, 65
 Shibuya, T., Ouchi, M., Harikane, Y., et al. 2017, *ArXiv e-prints*
 Silk, J. & Rees, M. J. 1998, *A&A*, 331, L1
 Sobral, D., Matthee, J., Darvish, B., et al. 2015, *ApJ*, 808, 139
 Stark, D. P., Ellis, R. S., Bunker, A., et al. 2009, *ApJ*, 697, 1493
 Stark, D. P., Ellis, R. S., Chiu, K., Ouchi, M., & Bunker, A. 2010, *MNRAS*, 408, 1628
 Stark, D. P., Richard, J., Charlot, S., et al. 2015, *MNRAS*, 450, 1846
 Stark, D. P., Richard, J., Siana, B., et al. 2014, *MNRAS*, 445, 3200
 Steidel, C. C., Rudie, G. C., Strom, A. L., et al. 2014, *ApJ*, 795, 165
 Stern, D., Dey, A., Spinrad, H., et al. 1999, *AJ*, 117, 1122
 Stroe, A., Sobral, D., Matthee, J., Calhau, J., & Oteo, I. 2017, *ArXiv e-prints*
 Talia, M., Brusa, M., Cimatti, A., et al. 2017, *MNRAS*, 471, 4527
 Talia, M., Mignoli, M., Cimatti, A., et al. 2012, *A&A*, 539, A61
 Taniguchi, Y., Kajisawa, M., Kobayashi, M. A. R., et al. 2015, *ApJ*, 809, L7
 Tasca, L. A. M., Le Fèvre, O., Hathi, N. P., et al. 2015, *A&A*, 581, A54
 Tasca, L. A. M., Le Fèvre, O., Ribeiro, B., et al. 2017, *A&A*, 600, A110
 Thacker, R. J., Scannapieco, E., & Couchman, H. M. P. 2006, *ApJ*, 653, 86
 Thomas, R., Le Fèvre, O., Scodreggio, M., et al. 2017, *A&A*, 602, A35
 Treu, T., Schmidt, K. B., Trenti, M., Bradley, L. D., & Stiavelli, M. 2013, *ApJ*, 775, L29
 Vanden Berk, D. E., Richards, G. T., Bauer, A., et al. 2001, *AJ*, 122, 549
 Vanzella, E., Pentericci, L., Fontana, A., et al. 2011, *ApJ*, 730, L35
 Villar-Martin, M., Tadhunter, C., & Clark, N. 1997, *A&A*, 323, 21

Table 2. Equivalent width of emission lines in stacked CIII] spectra

Line- λ	Sample							
	$EW(CIII)] \geq 20\text{\AA}$		$10 \leq EW(CIII)] < 20\text{\AA}$		$5 \leq EW(CIII)] < 10$		AGN type II	
	EW (\AA)	Flux (relative to CIII)]	EW (\AA)	Flux (relative to CIII)]	EW (\AA)	Flux (relative to CIII)]	EW (\AA)	Flux (relative to CIII)]
Ly α	71.7^{+4}_{-5}	4.6 ± 0.07	$58.8^{+7.0}_{-3.5}$	6.4 ± 0.04	$30.3^{+2.3}_{-1.5}$	5.2 ± 0.2	98.8^{+3}_{-3}	6.25 ± 0.06
NV- λ 1240Å	$0.9^{+0.3}_{-0.3}$	0.05 ± 0.02	$0.3^{+0.15}_{-0.15}$	0.02 ± 0.01	–	–	19.1^{+2}_{-2}	1.31 ± 0.1
SiII- λ 1309Å	$0.6^{+0.2}_{-0.2}$	0.07 ± 0.02	$0.2^{+0.15}_{-0.15}$	0.04 ± 0.02	–	–	$1.7^{+0.4}_{-0.4}$	0.12 ± 0.04
SiIV- λ 1403Å	$1.4^{+0.2}_{-0.2}$	0.13 ± 0.03	$0.1^{+0.15}_{-0.15}$	0.02 ± 0.02	–	–	$1.9^{+0.4}_{-0.5}$	0.14 ± 0.04
NIV- λ 1485Å	$2.2^{+0.3}_{-0.3}$	0.19 ± 0.02	$0.6^{+0.1}_{-0.1}$	0.08 ± 0.02	–	–	$2.5^{+0.5}_{-0.5}$	0.19 ± 0.05
CIV- λ 1549Å	$4.4^{+0.6}_{-0.5}$	0.31 ± 0.03	$2.4^{+0.5}_{-0.2}$	0.36 ± 0.02	$0.1^{+0.2}_{-0.3}$	0.01 ± 0.1	$38.8^{+2.0}_{-2.1}$	3.00 ± 0.08
HeII- λ 1640Å	$4.3^{+0.7}_{-0.4}$	0.27 ± 0.03	$3.2^{+0.5}_{-0.3}$	0.49 ± 0.03	$1.7^{+0.2}_{-0.2}$	0.3 ± 0.06	$11.7^{+1.0}_{-0.5}$	0.92 ± 0.06
OIII]- λ 1664Å	$5.5^{+0.6}_{-0.5}$	0.27 ± 0.03	$1.4^{+0.4}_{-0.3}$	0.14 ± 0.02	$0.7^{+0.2}_{-0.2}$	–	$1.7^{+0.6}_{-0.5}$	0.13 ± 0.05
NIII- λ 1750Å	$1.1^{+0.2}_{-0.2}$	0.07 ± 0.03	$0.4^{+0.2}_{-0.2}$	0.04 ± 0.02	–	–	$1.5^{+0.7}_{-0.6}$	0.13 ± 0.06
SiIII- λ 1888Å	$5.0^{+0.4}_{-0.3}$	0.18 ± 0.12	$4.0^{+0.4}_{-0.5}$	0.31 ± 0.10	–	–	$2.5^{+0.9}_{-0.8}$	0.19 ± 0.02
CIII]- λ 1908Å	$23.5^{+1.6}_{-1.8}$	1 ± 0.05	$11.1^{+1.2}_{-1.1}$	1 ± 0.04	$7.1^{+1.3}_{-1.1}$	1 ± 0.15	$13.2^{+1.2}_{-1.0}$	1.0 ± 0.09
UV slope β	-1.76 ± 0.08		-1.61 ± 0.03		-1.35 ± 0.02		0.09 ± 0.02	
$\Delta V_{outflow}$ km/s	1014 ± 205		445 ± 110		137 ± 61		–	

Table 3. Equivalent width of emission lines in stacked CIII] spectra

Line- λ	Sample			
	SFGs $2 < z < 3$		SFGs $3 < z < 4$	
	EW (\AA)	Flux (relative to CIII)]	EW (\AA)	Flux (relative to CIII)]
Ly α	$7.9^{+1.3}_{-1.3}$	3.5 ± 0.1	$14.8^{+1.5}_{-1.2}$	4.5 ± 0.12
CIV- λ 1549Å	$2.78^{+0.11}_{-0.06}$	-2.1 ± 0.05	$2.84^{+0.15}_{-0.05}$	-1.2 ± 0.05
CIII]- λ 1908Å	$2.0^{+0.2}_{-0.2}$	1 ± 0.05	$2.24^{+0.3}_{-0.2}$	1 ± 0.05
UV slope β	-0.94 ± 0.02		-0.92 ± 0.02	
$\Delta V_{outflow}$ km/s	65 ± 41		98 ± 40	